Kinetic investigation of K2CO3 as heat storage material

Biemans, Daan

Award date:
2017

Kinetic investigation of K_2CO_3 as heat storage material

Daan Biemans

2017-04

Supervisors:

Dr. ir. H.P. Huinink
MSc. L.C. Sögütoglu

TPM
TU/e

Abstract

In this project the reaction rate during hydration and dehydration cycles is investigated. The morphology of potassium carbonate particles changes while performing hydration-dehydration cycles. As a result both the hydration and dehydration rate increase asymptotically as a function of experienced cycles.

Also the vapor pressure dependency of the hydration as well as the dehydration process is investigated. Both processes do not occur at water vapor pressures close the equilibrium water vapor pressure. Using Arrhenius analysis an activation energy of (98 ± 2) kJ/mol K_2CO_3 is found.

The combination of the being a natural stabile system, having a storage density of 1.43 GJ/m^3 and having practical working conditions, makes potassium carbonate a promising material to be used as a heat storage material. However, storing potassium carbonate in the presence of CO_2 leads to formation of $KHCO_3$. No formation of potassium bicarbonate is observed during the experiments, only during storage. $KHCO_3$ dissociates when heating at 93 °C. No other side-products are observed in this project.

Table of content

Abstract 1
Table of content 2
1 Introduction 4
1.1 Thermal energy storage 4
1.2 Heat storage options 6
1.3 Hydrates 7
1.4 Typical seasonal heat storage system 8
1.5 Requirements of the material 10
1.6 Aim 11
1.7 Outline of the thesis 12
2 Theory 13
2.1 Phase lines 13
2.2 Nucleation and propagation 13
2.3 Classical nucleation theory 14
2.4 Kinetic curves 18
2.5 Arrhenius analysis 20
3 K_2CO_3: properties & chemistry 21
3.1 The K_2CO_3-H_2O-system 21
3.2 Molar enthalpies of reaction 22
3.3 K_2CO_3 in reactions 23
3.3.1 K_2O 24
3.3.2 KOH 25
3.3.3 $KHCO_3$ 26
4 Materials and methods 27
4.1 Material information 27
4.2 Thermogravimetric Analysis 29
4.3 Differential Scanning Calorimetry 30
4.4 Self-cooling & self-heating 31
5 Definitions & sample impurity 33
5.1 Defining loading and reaction speed 33
5.2 $KHCO_3$ impurity 34
5.2.1 Identification of the impurity 34
5.2.2 Consequences of the impurity 37
6 Hydration-dehydration cycling 38

6.1 Isothermal cycling – loading 38
6.2 Isothermal Cycling – heat 40
6.3 Temperature cycling 44
6.4 Discussion 47
7 Water vapor pressure dependency 49
7.1 Hydration 49
7.2 Dehydration 53
8 Conclusions & outlook 54
8.1 Conclusions 54
8.2 Outlook 55
9 Notation 56
10 References 58
11 Appendix 60
Appendix A: TGA Calibration 60
Appendix B: Error approximation 61
Appendix C: Flow-rate 62
Appendix D: Derivation of the Clausius-Clapeyron equation 64
Appendix E: Topley-Smith 65

1 Introduction

1.1 Thermal energy storage

Many colder countries consume more energy for heating than electrical power. An example is the Netherlands, where the major part of energy consumption is used for generation of heat, see figure 1.1a [1]. Currently, gas is the mostly used fuel for this purpose and thus also the main consumed resource, see figure 1.1b [2]. The growing interest in renewable energy, leads to demands of efficient renewable heat technologies like geothermal heating and solar thermal collectors. However, the use of geothermal heat is not optimal in the Netherlands. For instance, in Iceland temperatures over 200 °C are observed at roughly 1 km depth while in the Netherlands temperatures around 40 °C are measured at the same depth [3].

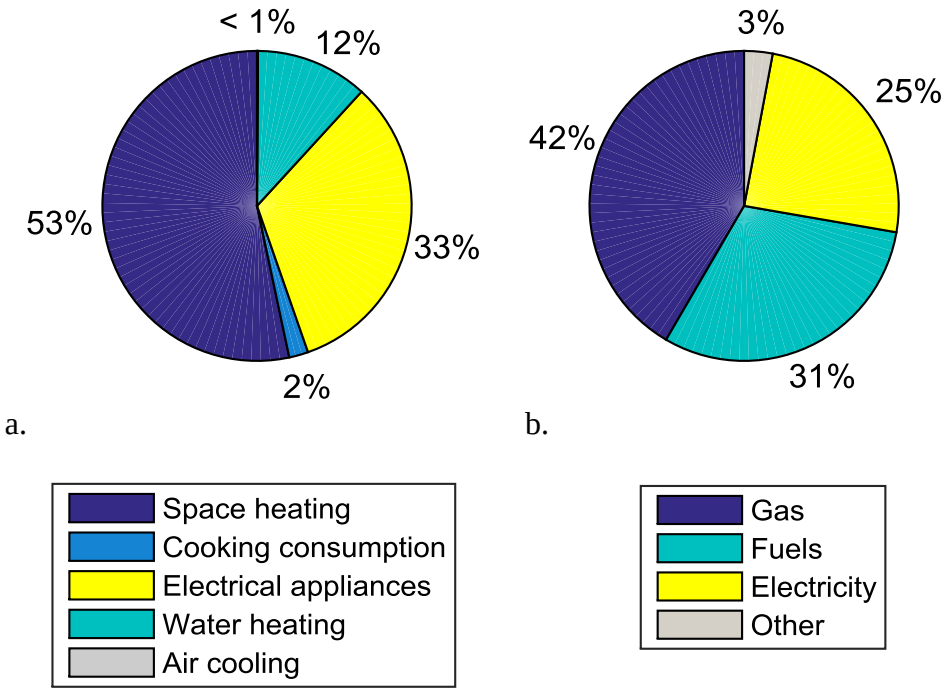

Figure 1.1. a: The energy consumption by end uses in the Netherlands in 2009 for the average household. b: The energy consumption by sources in the Netherlands in 2014 for the average household.

When using solar thermal energy another problem arises. During summer, the power provided by the sun is optimal, while the power demand is the highest during winter times. This difference between demand and supply is shown in figure 1.2 [2,4]. An efficient way of heat storage can solve the problem of a fluctuating energy production. The energy should be able to be stored in the summer, so that it can be used in the winter, when the energy production is much lower. Thermal energy storage is still in the stage of development.

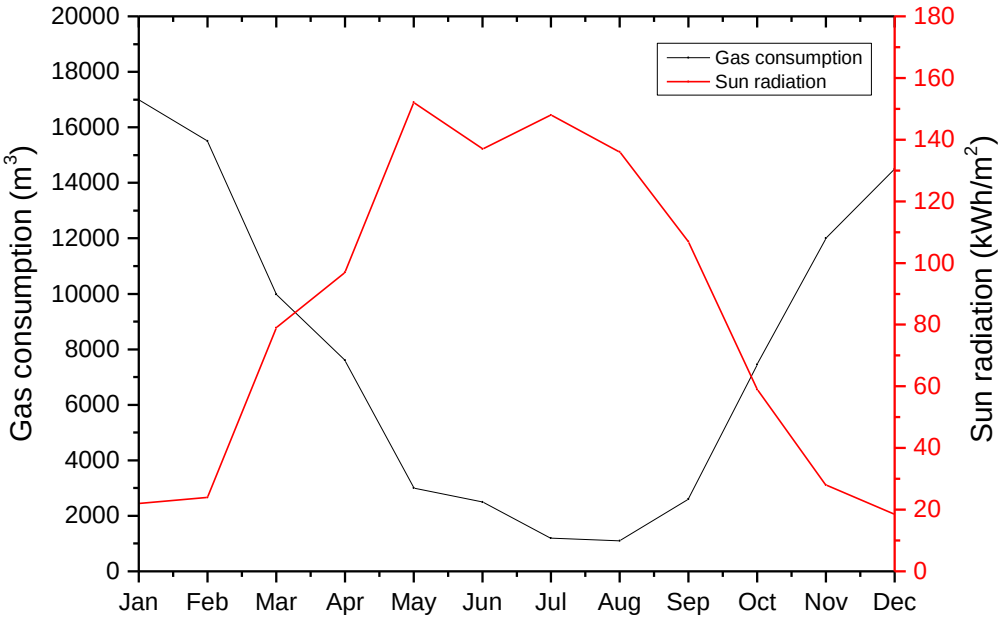

Figure 1.2. Difference between the gas consumption per household in the Netherlands and the power supply by the sun [2,4].

1.2 Heat storage options

In general, methods to store thermal energy are based on different aspects:

1. Heat capacity
   e.g. heating water and isolate the system, so the heat is still available at a later time.
2. Phase change materials (PCM's) and thermochemical materials (TCM's)
   In the latter energy is stored in chemical bounds using reversible chemical reactions.

Thermal heat storage based on heat capacity is for example used in 25 individual passive houses in Ireland [5]. Underground is a seasonal storage tank of 23 m^3 connected to solar collectors. The advantage of this method is that it is relatively easy to make and no expensive minerals are used. However, it also has its clear disadvantages. Firstly, constructing and isolating the water tank is quite an undertaking. The second reason is the low storage density (~0.2 GJ/m^3), which causes the need of large tanks: in cities this method is no option due to the lack of room. Furthermore, the variable discharging temperature and the large loss of heat (~45% after storing for one year) are clear downsides of this method [6].

The properties of thermal storage using PCMs and TCMs are clearly dependent on the used chemicals. Depending on the used chemicals heat can be stored in a wide temperature range, and the loss of heat can approach zero. PCMs are divided in two sub-categories: organic and inorganic compounds. Organic PCMs seem to be relatively stable, both from a mechanical and chemical point of view; meaning that the volume change is small and that the amount of side-reactions is insignificant. However, the downsides of organic PCMs are the low energy density (~0.2 GJ/m^3), the low thermal conductivity, their flammability and their high costs [7]. Inorganic PCMs have a better thermal conductivity and higher energy density (0.2-0.5 GJ/m^3) [7]. However, these materials show stability issues related to corrosion and incongruent melting.

Storage using thermochemical materials is based on physisorption or chemisorption. The first principle is based on adsorption of a liquid or gas by solids or liquids respectively. The fundamental interaction force is caused by the van der Waals force. Examples are silica gel and zeolites with corresponding energy densities of (0.12 GJ/m^3 and 0.25 GJ/m^3) [8]. TCMs based on chemisorption have a significant higher energy density, the formed bonds are covalent or ionic and thus stronger than the ones formed by physisorption. Materials from this category are salt hydrates, salt ammoniates and methanol complexes. All three have high energy densities which makes them suitable as heat storage materials. However, the fact that ammoniates and methanol complexes have higher flammability and toxicity values compared to salt hydrates favors the latter.

1.3 Hydrates

Hydrates are substances that contain water molecules integrated in their crystal structure. The general equation governing dehydration and its reverse reaction is given by:

$$\mathrm{MX} \cdot n\mathrm{H_2O} \leftrightharpoons \mathrm{MX} \cdot m\mathrm{H_2O} + (n-m)\mathrm{H_2O}, \tag{1.1}$$

Where $\mathrm{MX} \cdot n\mathrm{H_2O}$ is a crystalline hydrate with n water molecules in its lattice. When dehydrating m water molecules are released, decreasing the number of water molecules in the crystal lattice with the same amount. The dehydration reaction is endothermic, whereas its reverse reaction is exothermic and thus releases energy.

One could make a "heat battery" by controlling the reactions of a hydrate. This is done by changing the environmental conditions water vapor pressure and temperature. As an example, the phase diagram corresponding to the K_2CO_3-H_2O-system is shown in figure 1.3. When anhydrous potassium carbonate experiences an ambient water pressure p_w of 12 mbar corresponding to 10 °C, it heats up by following the equilibrium line until the given vapor pressure is reached, reaching a temperature of 60 °C. This heat can be extracted and used for further use. The now hydrated potassium carbonate can be dehydrated again by increasing the temperature or lowering the ambient vapor pressure.

The fact that the system works by controlling only these two parameters makes hydrates a promising candidate to use in heat storage applications. However, not every hydrate is suitable for practical use. Each hydrate has its own set of reaction conditions and properties. An overview of the requirements of the material is given in section 1.5.

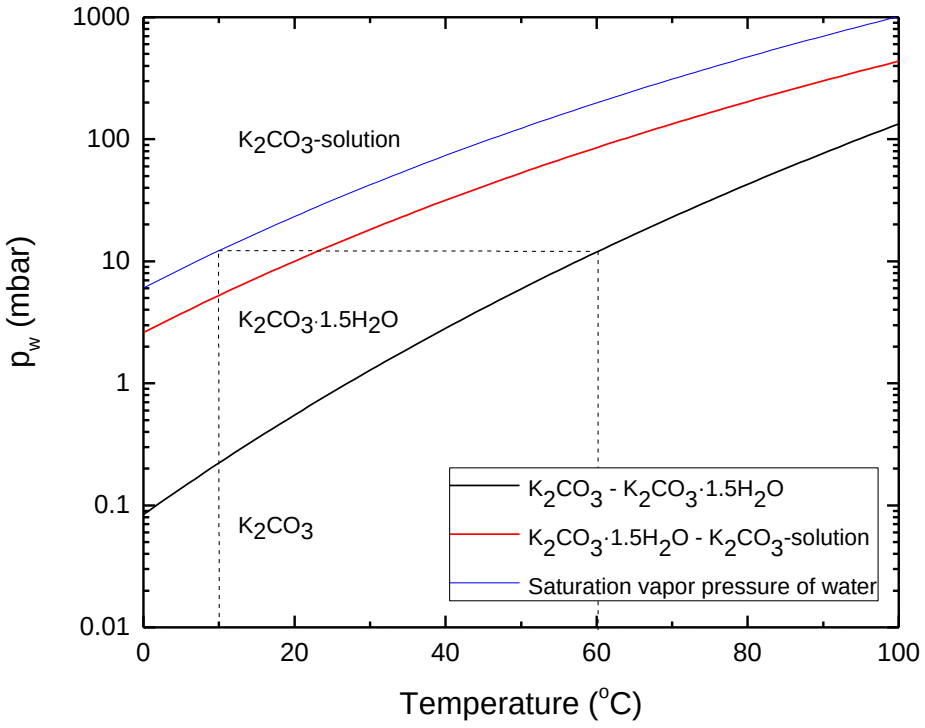

Figure 1.3. Phase diagram of K_2CO_3 in equilibrium with water. Experimental data from literature is extrapolated using the Clausius-Clapeyron relation [9].

1.4 Typical seasonal heat storage system

The general idea of a seasonal heat storage system by use of hydrates consists of two steps: dehydration and hydration. By controlling these respectively endothermic and exothermic reactions, heat can be stored during the hot seasons and extracted during colder times when heat is more needed.

The principle is explained on the basis of figure 1.4. During summer, the storage system is heated up using solar collectors. Solar collectors can heat the material up to around 150 °C [10], so it is necessary that the chosen material dehydrates before this maximum temperature is reached. The water that is released from the material by the dehydration process flows through a valve and condenses in a water compartment at 20-30 °C.

During winter, the water is evaporated in the water compartment and will flow through the valve to the material. The material now hydrates and due to the exothermic reaction: it heats up. This heat is extracted for further use, like domestic heating purposes. A water temperature of circa 10 °C is realistic in the Netherlands during winter. When higher water vapor pressures are needed, the water compartment has to be heated externally.

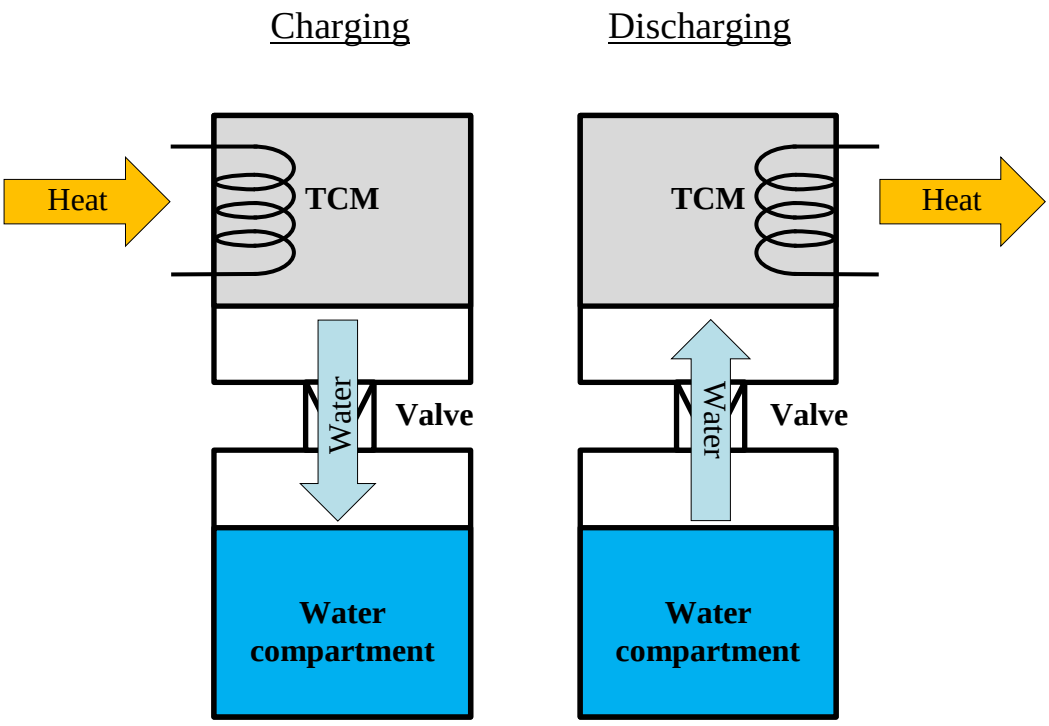

Figure 1.4. Charging and discharging principle of a closed system.

The system described above is a specific kind of system, namely a closed system. The system works with a water compartment, isolated from the atmosphere. In this way, the experimental conditions can be adjusted accurately and low pressures can be achieved [11].

The operating principle of an open system is shown in figure 1.5. When charging, dry hot air is blown through the TCM and dehydrates the material. When discharging, a humidifier is used to make cold wet air which is blown through the TCM. Due to the hydration process, the air warms up. The leaving hot (dry) air can be used for heating applications. The main advantage of an open system over a closed one is the lower cost of investment.

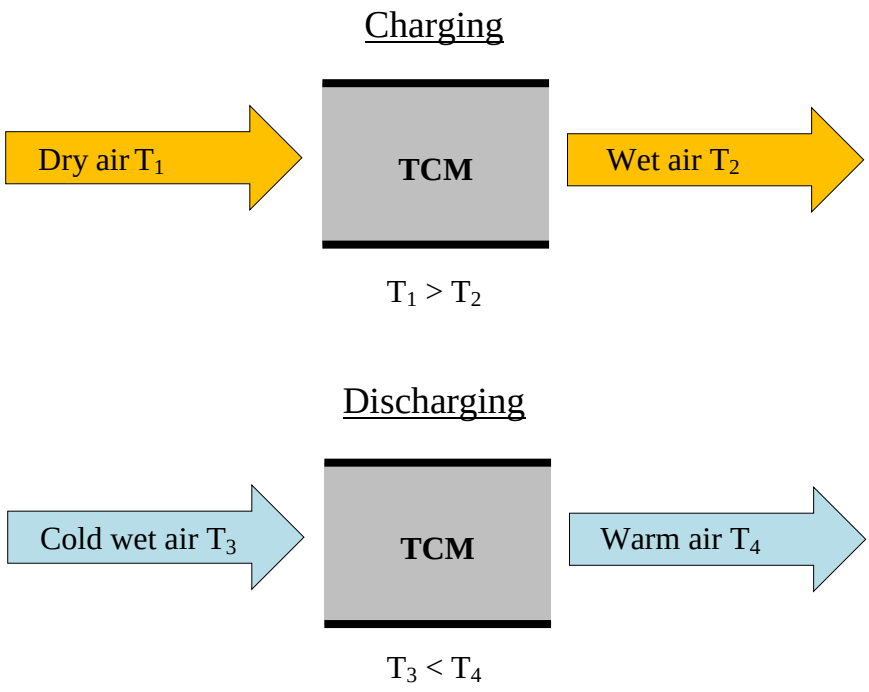

Figure 1.5. Charging and discharging principle of an open system.

1.5 Requirements of the material

Currently, the search of the most ideal material for a heat storage system is underway. The four most important requirements for the storage material are discussed in this paragraph: high storage density, system stability, costs and safety issues. Next, the eventual choice of material is discussed.

Storage density
The used material should not only have a high storage density but also have this at reasonable temperatures and water vapor pressures. Solar collectors can only heat the material up to around 150 °C and the material should be able to hydrate using a water compartment with a temperature of around 10 °C. Also, energy densities should be high enough compared to other storage options like zeolites and organic PCM's, which are in the order of 0.2-0.5 GJ/m^3.

Stability
The market, for example households, will not be interested in heat storage systems if it is only usable for a few cycles. Even if the system is very efficient, the inconvenience of replacing or maintaining a system with the associated costs will be the reason to not invest in a new heat storage system. The stated requirement is that the system should be stable for at least 30 cycles.

Costs
Costs are determined by two factors: the system design and the bulk storage material. However, the system design is also dependent of the type of storage material and its reaction conditions like ambient water vapor pressure.

Safety
Material safety is an important requirement when designing systems which are preferably going to be used in households. The material and any possible reaction products should be non-toxic and have a low inflammability.

Choice of material
No material is found yet that fulfills all needs naturally. Na_2S for example, has a high energy density, but is not safe for use in the residential environment due to its toxicity [12]. Another investigated salt is $MgCl_2$, its dehydration is accompanied by decomposition [13]. By making for example use of composites, storing the hygroscopic salt inside a porous matrix with open pores, this problem may be solved [14].

The salt investigated in this research project is K_2CO_3 and its hydrated form $K_2CO_3 \cdot 1.5H_2O$. The choice of material is based on a literature review performed on 563 salt hydrated reactions [15]. Although its energy density is relatively low: 1.43 GJ/m^3, compared with 1.93 GJ/m^3 for the magnesium dichloride hydrate, the material is still an interesting candidate due to its natural stability under multiple cycles. Modifying salts is preferably avoided because the fact that it decreases its energy density. Also its hydration and reverse reaction happen at practical temperatures (see phase diagram figure 1.3). The relatively low bulk price of €0.18 a kg and the lack of flammability and possible damage dealt to human health are also pros of the use of potassium carbonate.

1.6 Aim

Before designing a thermochemical reactor it is important to have sufficient information about the reaction kinetics and eventual side-reactions corresponding to the used thermochemical material. Dissociation of the thermochemical material leads to a decrease of the total storable heat. Furthermore, the formed product might limit the water vapor transport and decrease the reaction rate even more. The first aspect investigated in this project is the significance of any side-reactions under the conditions where the hydration and dehydration processes occur.

Dehydration and rehydration experiments by means of Thermogravimetric Analysis (TGA) are already performed using potassium carbonate by Stanish and Perlmutter [16-18]. Next, their most important observations are discussed, which give a raise to new questions regarding the use of potassium carbonate as a heat storage material.

Stanish and Perlmutter observed an increase of rehydration rate after experiencing one rehydration-dehydration cycle. Naturally, the magnitude of reaction rate is of importance for practical applications and thus, it is important to know how the material changes during cycling. In this project, the influence of cycling on the reaction speed is investigated using different particle sizes and morphologies by means of TGA and Differential Scanning Calorimetry (DSC). These observations are linked to the hypothesis which describes the behavior of potassium carbonate during hydration-dehydration cycling.

The results from Stanish and Perlmutter showed that the dehydration rate decays as a function of p_w/p_{eq} and reaches zero for $p_w/p_{eq} \approx 0.3$. Hydration rates were found to be very slow at pressures close to the equilibrium value for $p_w/p_{eq} < 1.5$ and become linear for $p_w/p_{eq} > 3$. These observations imply the need of a certain overpressure to cause any reaction. Solely from the phase diagrams one expects the hydration reaction already occurring at a water vapor pressure slightly above equilibrium. Analogously, dehydration would occur at water vapor pressures slightly below equilibrium. In order to improve understanding of their results, similar experiments are performed during this project using the TGA technique and coupled with classical nucleation theory.

1.7 Outline of the thesis

Theory

The thesis starts with a theoretical section, wherein the concepts nucleation and propagation are introduced. Next, classical nucleation theory is used to describe the nucleation step of the hydration process. Furthermore, the shape of kinetic curves is discussed shortly. Finally, the method used to analyze the water vapor dependency measurements is described.

K_2CO_3: properties & chemistry

All relevant information about the used hydrate, potassium carbonate, is given in this chapter. The hydration-dehydration reaction is discussed and possible side reactions are evaluated.

Materials & methods

In this chapter more detailed information is listed about the used potassium carbonate samples, i.e. size, supplier and way of storage. Also, the used TGA and DSC techniques are discussed shortly. Finally, the significance of self-cooling and self-heating during the experiments is investigated.

Definitions & sample impurity

The chapter starts by defining the concepts of loading and reaction rate. Some experiments are performed using partially impure samples. Proof of the nature of the impurity and its relevance is also discussed in this chapter.

Hydration-dehydration cycling

In this chapter the behavior of potassium carbonate during dehydration-hydration cycles is investigated. Hydration and dehydration rates of different particle sizes are compared using experimental data. Also the influence on the reaction speed of particle morphology is investigated.

Vapor pressure dependency

In the last chapter the vapor pressure dependency of the hydration as well as the dehydration process is investigated. Experimental data is coupled with thermodynamic theory for this purpose.

2 Theory

At first, the Clausius-Clapeyron equation corresponding to a hydrate system is given. Next, the phenomena nucleation and propagation are discussed generally. In the third section, classical nucleation theory is used to describe the nucleation rate corresponding to the hydrate process at different water vapor pressure and temperatures. Next, experimental kinetic curves are compared to the ones obtained using the spherical shrinking model. Finally, the temperature dependency of the hydration rate is evaluated by Arrhenius analysis.

2.1 Phase lines

The Clausius-Clapeyron relation is useful for constructing phase diagrams. Given the enthalpy of evaporation and the vapor pressure at a certain temperature, one can predict the vapor pressure at any given point. The derivation is shown in Appendix D. The Clausius-Clapeyron equation for a hydrate system is given by:

$$\frac{\mathrm{d}\ln p_{eq}}{\mathrm{d}\left(\frac{1}{T}\right)} = \frac{\Delta H}{(m-n)R_g}, \tag{2.1}$$

where p_{eq} is the equilibrium water vapor pressure between the two hydrate phases [mbar], T is the temperature [K], $(m\text{-}n)$ the amount of water molecules reacting, R_g is the gas constant [$J \cdot mol^{-1} \cdot K^{-1}$] and ΔH_w *is* the enthalpy change per mole H_2O [J/mol]. The amount of water molecules reacting is in the case of potassium carbonate equal to 1.5. The phase diagram in figure 1.3 is constructed by extrapolating data points from literature using the Clausius-Clapeyron relation [9].

2.2 Nucleation and propagation

Most studies about crystalline hydrates investigate the dehydration process. Even though this reaction is reversible, it does not mean that both dehydration and rehydration have the exact same characteristics. Both reactions are dependent on multiple factors like particle size, reaction surface, temperature and water vapor pressure which influences the processes differently. The total reaction process is characterized by the combination of two processes: nucleation and propagation. These will be discussed in this section in more detail.

Nucleation is often initiated in damaged regions. For this reason experiments lead sometimes to irreproducible results. Even when the sample is prepared with such care, unavoidable variations in defect structure from one crystal to another may lead to different results. So the induction period of nucleation does not only depend on the experimental conditions, but also on the sample itself. A more perfect particle can have a much longer induction period compared to a cracked particle. Also, the rate of continuation of nucleation is not constant. During dehydration of $CuSO_4 \cdot 5H_2O$, the number of nuclei turned out to be increasing linear with time [19], while the formation of nuclei corresponding to the dehydration of $NiSO_4 \cdot 7H_2O$ seemed to increase with t^2 [20].

Nuclei grow and propagation occurs. Maybe the most important feature of this stage is the influence of the reaction product layer on the water transport. The impact of this effect is often referred to as “impedance”. Due to impedance, a reaction can sometimes not complete, even when it is placed under conditions far from equilibrium. In most cases, the reaction is initially limited by nucleation and after a

while, propagation becomes relatively more important and will eventually become the limiting factor.

2.3 Classical nucleation theory

Classical nucleation theory is used in an attempt to give more insight into hydration processes at different temperatures or pressures. The generic expression for the nucleation rate J [mol/s] is given by [21]:

$$J = N_s \beta Z \, exp\left(-\frac{\Delta G^*_{nucl}}{k_B T}\right), \tag{2.2}$$

where,

N_s: number of nucleation sites [-]
β: rate at which molecules attach to the nucleus causing it to grow [mol/s]
Z: Zeldovich factor (probability that the nucleus forms the new phase, not dissolves) [-]
ΔG^*_{nucl}: change in Gibbs free energy corresponding to a critical nucleus [J]
k_B: Boltzmann constant [J·K^{-1}]

All terms in this expression will be validated for the nucleation of a hydrate system. At first, the exponent, which denotes the chance of forming a nucleus, will be derived. Secondly, the pre-factors will be discussed and eventually the rate will be plotted as function of the vapor pressure at different temperatures.

The total change in Gibbs free energy by formation of a nucleus is given by the sum of a bulk term and a surface term:

$$\Delta G_{nucl} = \Delta G_{bulk} + \Delta G_{surface}. \tag{2.3}$$

The bulk term is dependent on the amount of mole present in a nucleus, N [mol], the bulk terms g_i [J/mol] for phases n and m, and the bulk term of the gas corresponding to the reaction:

$$\Delta G_{bulk} = N(g_n - g_m) - N(n-m)\mu_w^{gas}, \tag{2.4}$$

where μ_w^{gas} [J/mol] denotes the chemical potential of the water vapor and the bulk terms g_i are given by the sum of the corresponding chemical potential $\mu_{s,i}$ [J/mol] and the amount of water molecules per mole hydrate times the chemical potential μ_w [J/mol]:

$$g_n = \mu_{s,n} + n\mu_w, \tag{2.5}$$

and

$$g_m = \mu_{s,m} + m\mu_w. \tag{2.6}$$

When phases n and m are in equilibrium, their chemical potentials are equal: $\mu_{s,n} = \mu_{s,m}$. This means that the total bulk term is only dependent of the amount of water molecules involved during the process and their change of chemical potential: $\Delta\mu_w$ [J/mol].

$$\Delta G_{bulk} = N(n-m)\left[\mu_w - \mu_w^{gas}\right] = N(n-m)\Delta\mu_w. \tag{2.7}$$

Using $\Delta\mu_w = -R_g T \ln\left(\frac{p_w}{p_{eq}}\right)$, the total bulk term is given by:

$$\Delta G_{bulk} = -N(n-m)\, R_g T \ln\left(\frac{p_w}{p_{eq}}\right). \quad (2.8)$$

The surface terms are evaluated using the following model: a half-spherical nucleus is formed on the vapor-crystal surface, see figure 2.1. The change in contact surface with air due to the size difference between a *m* and *n* hydrate is neglected. This means that the surface term is equal to the surface energy $\gamma_{m,n}$ [J/m^2] times the area *A* [m^2] of the nucleus touching the m-phase:

$$\Delta G_{surface} = \gamma_{m,n}\, A. \quad (2.9)$$

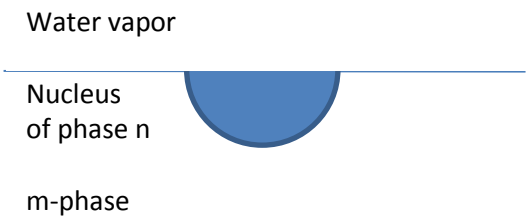

Figure 2.1. The used nucleation model: a half-spherical nucleus is formed on the vapor-crystal surface.

The area *A* can be expressed as a function of the number of particles inside the nucleus. The area is equal to the area of a half sphere with nucleus radius r_{nucl} [m], which is expressible in the nucleus volume V_{nucl} [m^3]. By substituting the nucleus volume by the product of the molar volume of the n-phase crystal v_n [m^3/mol] and the amount of moles present in the nucleus, the following expression is found for the area *A*:

$$A = 2\pi r_n^2 = 2\pi\left(\frac{3V_n}{2\pi}\right)^{\frac{2}{3}}, \quad (2.10)$$

where $V_{nucl} = v_n N$ and thus the area in terms of *N* is given by:

$$A = 2\pi\left(\frac{3v_n}{2\pi}\right)^{\frac{2}{3}} N^{\frac{2}{3}}. \quad (2.11)$$

To make the expression of the total change in Gibbs free energy more clear, the terms independent of *N* are substituted by C_1 [J/mol] and C_2 [J/mol$^{2/3}$]:

$$C_1 \equiv (n-m)\, R_g T \ln\left(\frac{p_w}{p_{eq}}\right), C_2 \equiv 2\pi\left(\frac{3v_n}{2\pi}\right)^{\frac{2}{3}} \gamma_{m,n}. \quad (2.12)$$

Resulting in:

$$\Delta G_{nucl} = -C_1 N + C_2 N^{2/3}. \quad (2.13)$$

By differentiating this term with respect to *N* the amount of moles present in a critical nucleus can be found, N^*. Nuclei with less particles are not likely to since an increase in particles leads to an increase in Gibbs free energy.

$$\frac{d(\Delta G)}{dN} = -C_1 + \frac{2}{3} C_2 N^{-\frac{1}{3}} = 0 \quad (2.14)$$

$$N^* = \left(\frac{2C_2}{3C_1}\right)^3 \tag{2.15}$$

The change in Gibbs free energy corresponding to the formation of a critical nucleus is denoted as ΔG^*_{nucl}, which is the term in the exponent of the rate equation. In terms of p_w/p_{eq}:

$$\Delta G^*_{nucl} = \frac{4C_2^3}{27}\left((n-m)R_gT\ln\left(\frac{p_w}{p_{eq}}\right)\right)^{-2}$$

The next step is evaluating the pre-factors. N_s corresponds to the number of nucleation sites and thus is dependent on the sample itself. When assuming the sample stays the same at different temperatures, N_s is constant. The exact values belonging to this pre-factor is hard to derive, but when comparing the dependency of the nucleation rate on the water vapor pressure at different temperatures, the exact value is not needed. β is the rate of the nucleus growth; the exact expression for β is hard to derive, it might be a function of p_w and/or the temperature. The experimental results are evaluated by assuming β to be independent of the ambient water vapor pressure, but dependent of the temperature, see chapter 7. Calculations in this chapter are performed by assuming both pre-factors to be equal to unity.

The last pre-factor is called the Zeldovich factor Z [34], which corresponds with the probability will indeed form the new phase. The definition of the Zeldovich non-equilibrium factor is:

$$Z = \sqrt{\frac{-1}{2\pi R_gT}\frac{\partial^2\Delta G^*}{\partial N^{*2}}}, \tag{2.16}$$

which in the case of the hydrate system simplifies to:

$$Z = \sqrt{\frac{1}{2\pi R_gT}\frac{2}{9}C_2N^{*-4/3}}\,. \tag{2.17}$$

In terms of p_w/p_{eq}:

$$Z = \sqrt{\frac{9}{16\pi R_gTC_2^3}}\left((n-m)R_gT\right)^2\left(\ln\left(\frac{p_w}{p_{eq}}\right)\right)^2. \tag{2.18}$$

Now all factors are evaluated, it is possible to rewrite the expression of the nucleation rate in terms of T and p_w/p_{eq}:

$$J = a\,T^{\frac{3}{2}}\left(\ln\left(\frac{p_w}{p_{eq}}\right)\right)^2\exp\left(-b\,T^{-3}\left(\ln\left(\frac{p_w}{p_{eq}}\right)\right)^{-2}\right), \tag{2.19}$$

wherein a [mol·s^{-1}·K$^{-3/2}$] and b [K^3] are defined by:

$$a \equiv N_s\beta\sqrt{\frac{9}{16\pi R_gC_2^3}}\left((n-m)R_g\right)^2, \qquad b \equiv \frac{4C_2^3}{27k_B\left((n-m)R_g\right)^2}. \tag{2.20}$$

Expression 2.19 is used to fit the experimentally obtained hydration rate data at fixed temperatures in chapter 7, a and b are the fitting parameters.

Next, the magnitude of ΔG^*_{nucl} is calculated for different pressure ratios p_w/p_{eq}. The parameters used correspond to the potassium carbonate system. However, the magnitude of the surface energy $\gamma_{m,n}$ is not known. To make an approximation, the surface energy for NaCl is used, which is of the order 0.3 J/m^2 [22]. However, using this value, the calculated magnitude of ΔG^*_{nucl} is so high, see figure 2.2a, that the nucleation rate is approximate zero under the given conditions. In figure 2.2b, ΔG^*_{nucl} is shown corresponding to a surface energy of a factor ten lower. The corresponding nucleation rate as a function of the pressure ratio p_w/p_{eq} is shown in figure 2.3. Here, the behavior of the nucleation rate is visible: its magnitude remains approximate zero until a certain pressure ratio is reached and then increases rapidly.

The point where the nucleation rate starts increasing significantly is dependent of the surface energy. Measuring the surface energy accurately is quite an undertaking, because it also depends on the crystal structure. A reaction will most likely favor a specific direction instead of proceeding uniformly. This also points out a major flaw in the above model, where the nucleus is formed onto the vapor-crystal surface without having any consequences caused by crystal structure.

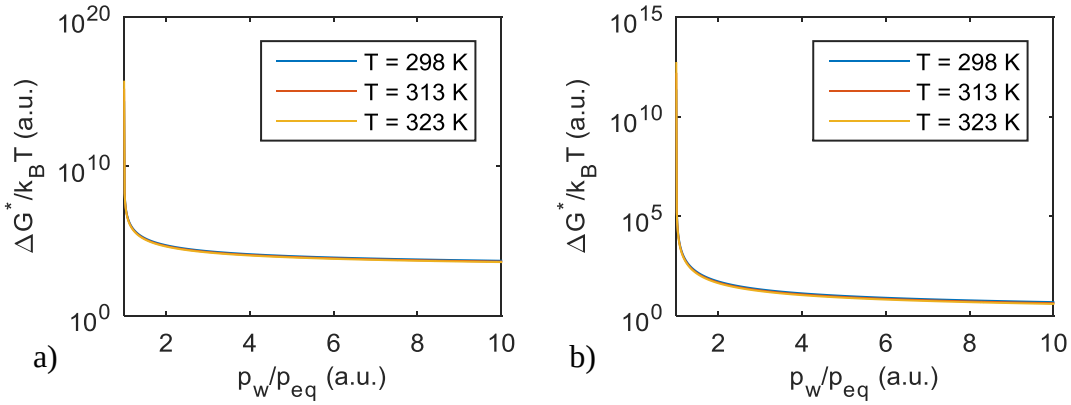

Figure 2.2. The change in Gibbs free energy corresponding to a critical nucleus for the hydration process of potassium carbonate for a: $\gamma_{m,n}$ = 0.3 J/m^2 and b: $\gamma_{m,n}$ = 0.03 J/m^2.

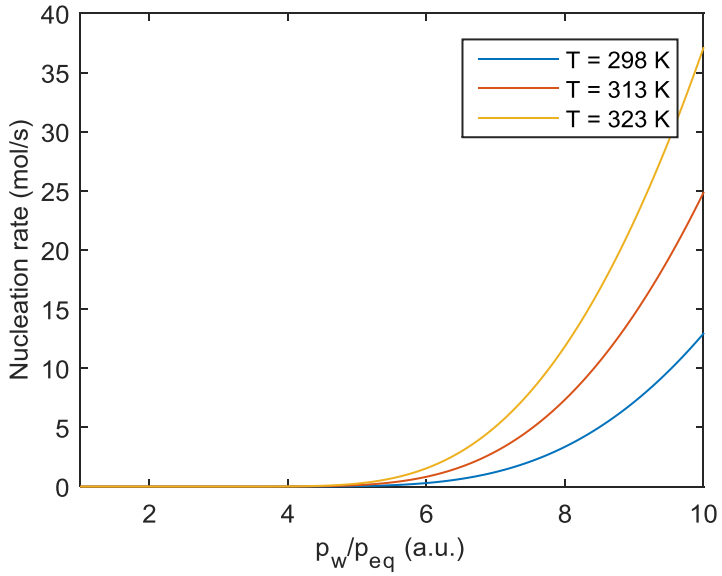

Figure 2.3. The nucleation rate corresponding to the hydration process of potassium carbonate for: $\gamma_{m,n}$ = 0.03 J/m^2, N_s = 1 and β = 1 mol/s.

2.4 Kinetic curves

In the past, many attempts have been made to model dehydration processes with varying results. Most of these models assume a constant reaction interface rate. However, this assumption is by far not viable for every material and/or in every condition, so modifications are needed. Next, the spherical shrinking model will be explained and its shortcomings will be appointed [23].

Assume a spherical particle where the outer layer grows during time, so the inner unreacted core shrinks, see figure 2.4. Using this model, the rate of conversion X is found by dividing the volume of the core by the total volume of the particle:

$$1 - X = \frac{\frac{4}{3}\pi r_c^3}{\frac{4}{3}\pi R^3} = \left(\frac{r_c}{R}\right)^3, \tag{2.21}$$

where R is the total radius of the particle and r_c the radius of the unreacted core [m].

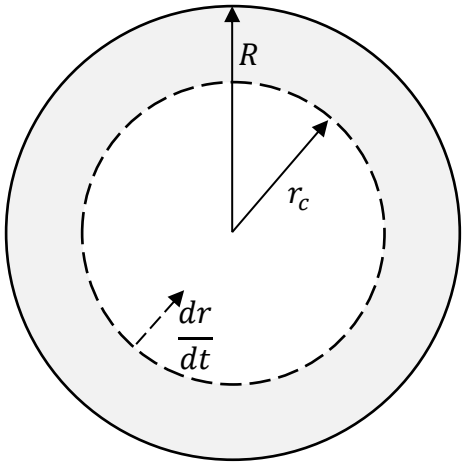

Figure 2.4. Spherical shrinking model. A hydrated particle with radius R has a unreacted core with a radius r_c, the shrinking rate is assumed to be constant.

When assuming the shrinking rate dr/dt to be constant, one can write the reaction rate equation as function of time:

$$1 - X = \left(\frac{R - \frac{dr}{dt}t}{R}\right)^3, \tag{2.22}$$

resulting in:

$$X = 1 - \left(1 - \frac{dr}{dt}\frac{t}{r_0}\right)^3. \tag{2.23}$$

This function of conversion rate is plotted in figure 2.5 together with a typical kinetic curve for dehydration. The latter is based on experimental data of isothermal dehydration of $K_2CO_3 \cdot 1.5H_2O$ at 48 °C with no water vapor present.

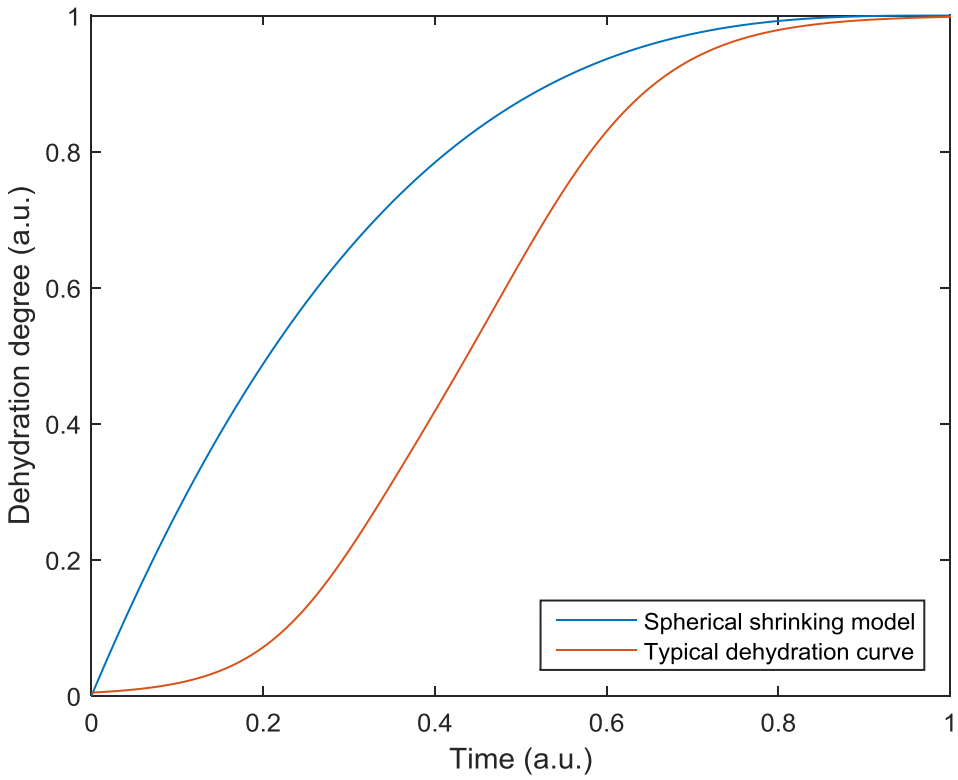

Figure 2.5. Kinetic curve obtained using the spherical shrinking model compared to a typical dehydration curve, obtained from isothermal dehydration experiments at 48 °C of $K_2CO_3 \cdot 1.5H_2O$ with no water vapor present.

From comparing real data with the model one can conclude that not enough aspects are considered. To make a better model, modifications are needed. The initial growth is significantly less than predicted, the influence of the induction period must be taken into account. Secondly, the rate of reaction interface advance doesn't have to be constant, it may vary with crystallographic direction. And thirdly, the impedance effect caused by the product layer may limit water transport, this effect varies possibly with the ambient water vapor pressure. It should be taken in mind that the noted points could be temperature dependent as well.

2.5 Arrhenius analysis

The sign of the change in Gibbs free energy ΔG gives information about whether the reaction is favored or not, i.e. a negative value of ΔG corresponds to a favored reaction, while a positive value implies an unfavorable reaction. The Gibbs free energy in a closed system is given by:

$$dG = Vdp - SdT. \tag{2.24}$$

The system is assumed to be in vacuum, which implies that the ambient pressure is fully determined by the water vapor pressure p_w. If the temperature is constant, above equation can be integrated with respect to p, resulting in:

$$G(p_w) - G(p_{eq}) = \int_{p_{eq}}^{p_w} Vdp. \tag{2.25}$$

V is defined by the volume of the total system, i.e. the volume of the solid hydrate and the volume of the gas involved. The volume of the solid phase is very small compared to the volume of the gas. Approximating the volume of the solid phase as zero and expressing the gas volume in terms of p_w (ideal gas law), results in the following expression for the change in Gibbs free energy:

$$\Delta G = G(p_w) - G(p_{eq}) = -nR_gT \ln\left(\frac{p_w}{p_{eq}}\right), \tag{2.26}$$

which means that the driving force (ΔG) is dependent of the temperature and p_w/p_{eq}. For this reason, the hydration rate is estimated as a product of a temperature-dependent term $k(T)$ [mol/s] and a term dependent of the pressure ratio $f(p_w/p_{eq})$ [-]:

$$Hydration\ rate \approx k(T) f\left(\frac{p_w}{p_{eq}}\right). \tag{2.27}$$

The temperature dependency of the reaction rate can be estimated using the Arrhenius equation [24]:

$$k(T) = A \exp\left(-\frac{E_a}{R_gT}\right), \tag{2.28}$$

where A_0 is the collision rate [mol/s] and E_a the activation energy [J/mol]. When $f(p_w/p_{eq})$ is known, the hydration rate data can be fitted by using eq. 2.27 to obtain the activation energy. This method is used in section 7.1. As a check if the made assumptions are justified, the hydration rate should be divided over the exponential term, resulting in a master curve describing the hydration process independently of the temperature.

3 K_2CO_3: properties & chemistry

In this chapter an overview is given about relevant information about potassium carbonate as a TCM. At first, the K_2CO_3-system and its corresponding hydration-dehydration reaction equation is discussed. Secondly, the corresponding molar reaction enthalpy is obtained. Finally, possible side reactions causing impurities in the material are evaluated.

3.1 The K_2CO_3-H_2O-system

In this project, the possible use of potassium carbonate in heat storage applications is investigated. This white salt is soluble in water and when deliquescent it becomes a clear solution. At room temperature its equilibrium relative humidity is ~43% [25]. The corresponding reversible dehydration reaction equation is given by:

$$K_2CO_3 \cdot 1.5H_2O(s) \leftrightharpoons K_2CO_3(s) + 1.5H_2O(g). \quad (3.1)$$

By looking at this reaction equation, two things can be concluded. The first remark is that there are only two states, no intermediate state is formed during the process. This is without a doubt a pro for practical uses: besides the fact that the existence of an intermediate complicates the system, it may also decreases the reaction rate significantly or reduce the overall output power. This is for example the case in the $MgSO_4$-system. Here, transition of $MgSO_4 \cdot 7H_2O$ to the corresponding hexahydrate already occurs (slowly) at 25 °C, decreasing the output of the reactor. [26].

The second observation we made is that the hydrated form only contains a loading of 1.5 water molecules. This is a con of using K_2CO_3, because it implies that the reaction enthalpy, and thus heat storable in the system, is low compared to for example $MgCl_2$, which can store up to 6 water molecules. It should be noted down that this method of qualification is not completely fair. For practical uses, the energy density per volume is more useful than per mole. Using 97.1 kJ/mol K_2CO_3, obtained by DSC experiments shown in section 3.2, gives an energy density of 1.43 GJ/m^3 based on the density and molar mass of the sesquihydrate. Which is a relatively low number compared to other hydrates, but still around a factor 7 higher compared to heat storage systems based on heat capacity.

An important need a material must fulfill is that the reactions happen at practical conditions. On basis of the phase diagram shown in figure 1.3 it is visible that the K_2CO_3-H_2O system fulfills the practical conditions as discussed earlier. Dehydration occurs below temperatures of 150 °C, which is the maximum achievable temperature by making use of solar collectors. Hydration should occur at ambient water vapor pressures p_w < 12 mbar. High water vapor pressures can be achieved by heating up a water bad, which costs energy and thus should be avoided as much as possible.

3.2 Molar enthalpies of reaction

The molar enthalpies of the hydration and dehydration processes are obtained in two different ways. Firstly, by making use of eq. 2.1 and the equilibrium data from literature [9]. By plotting the natural logarithm of the equilibrium vapor pressure against the reciprocal of the temperature and fitting using a linear fit the molar enthalpy change is determined: ΔH = (93.7±1.2) kJ/mol K_2CO_3.

Another way to determine the molar enthalpy change is by simply measure it during a DSC experiment, see figure 3.1. The initial sample consists of 6.5 mg $K_2CO_3 \cdot 1.5H_2O$ and is placed in an open aluminum sample holder. The water vapor pressure is kept constant at 10 mbar and the imposed temperature is 25 °C during hydration and 100 °C when dehydrating. Like during isothermal DSC experiments, no significant difference between the enthalpies corresponding to the number of performed cycles is observed. There is a slight difference between the hydration enthalpy and the dehydration enthalpy present i.e. (97.1±0.2) kJ/mol K_2CO_3 compared to (98.8±0.5) kJ/mol K_2CO_3. These values are obtained by averaging over ten dehydration-hydration cycles.

The molar enthalpy change obtained from the Clausius-Clapeyron equation is slightly lower than the experimental values. However, due to the fact that the difference is relatively small, one can conclude that the Clausius-Clapeyron is applicable as a guideline to the K_2CO_3 hydrate system as expected.

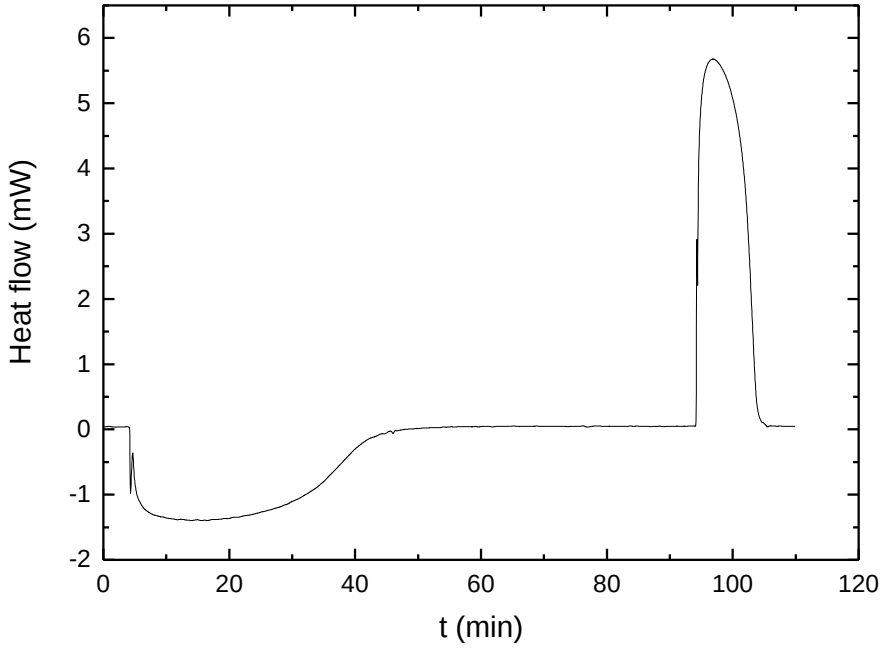

Figure 3.1. DSC peaks of dehydration and hydration of potassium carbonate. The integrals over the peaks correspond to the dehydration enthalpy (negative peak) and hydration enthalpy (positive peak).

3.3 K_2CO_3 in reactions

It is important to prevent any dissociation, or at least minimize it, to make sure no wrong conclusions are drawn from any TGA measurements. The presence of any side-reactions could result in an overestimation (or underestimation) of the observed reaction rate. For practical use the presence of any reactions is of course also not wanted, it could lead to a decrease of the heat storage capacity of the reactor. Furthermore, dissociation reactions may also result in products that damage the storage system. For example, for chloride salts, HCl may be formed at higher temperatures, which is corrosive and thus damages the storage system [27].

In this section, the most probable reactions of potassium carbonate in combination with the used environmental conditions are discussed. Firstly, it is shown that the formation of K_2O and KOH can be excluded by means of calculating the equilibrium conditions of the corresponding reaction. Secondly, the conditions corresponding to formation of $KHCO_3$ are discussed and it is shown that potassium bicarbonate is possibly a stable state during the experimental conditions. Dissociation of $KHCO_3$ would lead to CO_2 outgassing and thus formation of potassium carbonate.

Equilibrium conditions for constructing phase diagrams are calculated by using the following equations [28]:

$$\alpha A(s) + \beta B(g) \leftrightharpoons \gamma C(s) + \delta D(g), \tag{3.2}$$

and

$$\Delta_r G(T) = \Delta_r G^0(T) + R_g T ln\left(\frac{p_A^\alpha \cdot p_D^\delta}{p_C^\gamma \cdot p_B^\beta}\right), \tag{3.3}$$

where $\Delta_r G$ is the reaction Gibbs energy, $\Delta_r G^0$ the standard reaction Gibbs energy and p_i denotes the vapor pressures of molecule i and is equal to 1 for a solid. When the reaction Gibbs energy turns out to be negative, the forward reaction is favored. When positive, the backwards reaction is favorable. In its equilibrium, the reaction Gibbs energy is equal to zero. When constructing phase diagrams, $\Delta_r G^0(T)$ should be known. Lehman et al. [28] investigated the reactions associated with K_2O and KOH and give an empirical formula to compute $\Delta_r G^0(T)$ for these reactions. For the reaction corresponding to $KHCO_3$, static data provided by Wagman et al. of the enthalpy and entropy is used to compute $\Delta_r G^0(T)$ [29].

3.3.1 K_2O

The decomposition reaction corresponding to potassium carbonate is given by:

$$K_2CO_3(s) \leftrightharpoons K_2O(s) + CO_2(g). \quad (3.4)$$

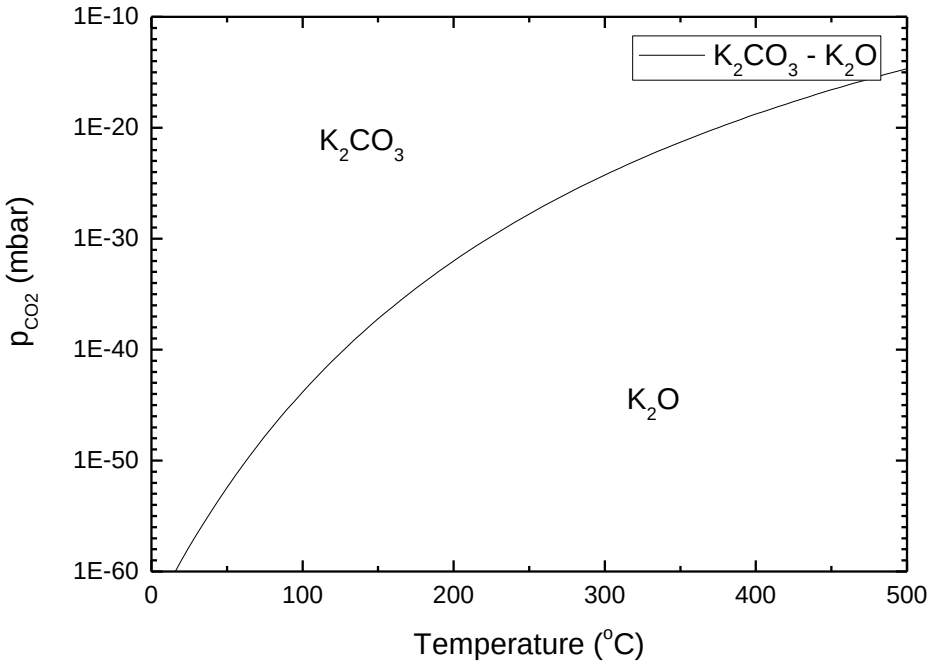

Figure 3.2. Phase diagram of K_2O in equilibrium with CO_2.

As visible in the phase diagram in figure 3.2, the decomposition reaction will occur at very low vapor pressures of CO_2. The vapor pressure of CO_2 during storage will be in the order of 0.4 mbar, so no decomposition will happen. Even in the case of a closed reactor under vacuum it is unrealistic that such low pressures will be reached.

3.3.2 KOH

Potassium carbonate is produced by means of carbonating potassium hydroxide. When the CO_2 vapor pressure is low enough, the reverse reaction is possible:

$$\mathrm{KOH(l) + CO_2 \leftrightharpoons K_2CO_3(s) + H_2O(g).} \qquad (3.5)$$

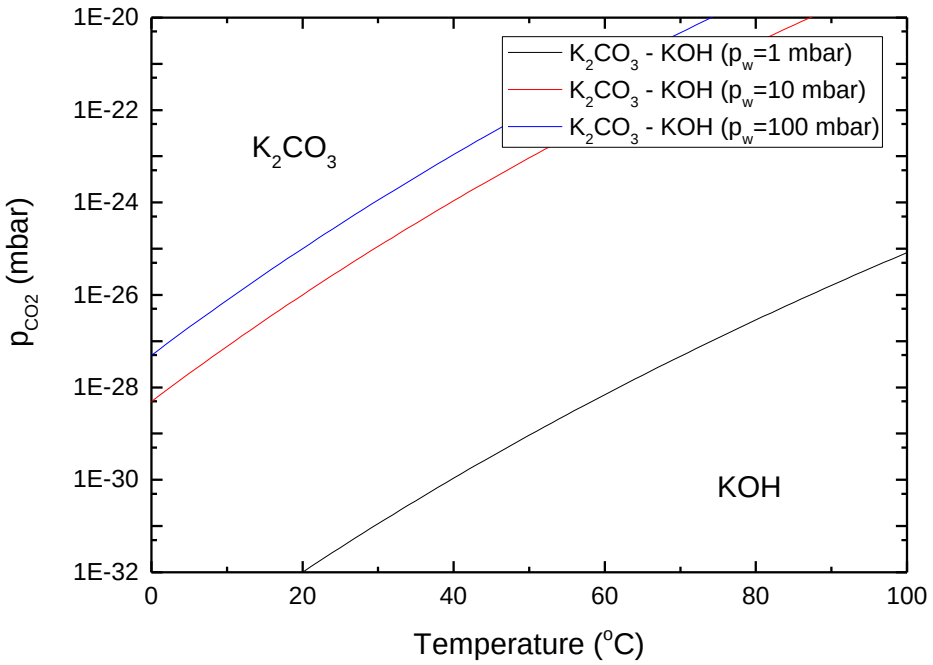

Figure 3.3. Phase diagram of KOH in equilibrium with CO_2 for different water vapor pressures.

Even though this reverse reaction is favored for higher CO_2 pressures than is needed for the formation of K_2O, it is still very low, see figure 3.3. Thus, the decomposition of potassium carbonate is not significant during the experiments, nor in a reactor.

3.3.3 $KHCO_3$

Potassium bicarbonate is a reaction product of potassium carbonate and CO_2. As well as the anhydrate as the hydrate are possible reactants:

$$K_2CO_3(s) + H_2O(g) + CO_2(g) \leftrightharpoons 2KHCO_3(s), \quad (3.6)$$

and

$$K_2CO_3 \cdot 1.5H_2O(s) + CO_2(g) \leftrightharpoons 2KHCO_3(s) + 0.5H_2O(g). \quad (3.7)$$

Static enthalpy and entropy data from Wagman et al. is used in to make the phase diagram corresponding to the $KHCO_3$-K_2CO_3-K_2CO_3·$1.5H_2O$-system as shown in figure 3.4. The colors indicate the stable materials according to the phase diagram.

During storage at room conditions, formation of potassium bicarbonate is observed. When heating at 93 °C, the potassium bicarbonate turns into potassium carbonate, see section 5.2. This behavior matches with the expectations according to the phase diagram. However, no increase of $KHCO_3$ is observed during any experiment, which indicates that the corresponding rate of reaction rate is insignificant compared to the hydration and dehydration rates. Also the fact that the potassium bicarbonate is observed as a stable state at a temperature of 48 °C is in contradiction with this phase diagram. The contradictions are shown in more detail in chapter 5.

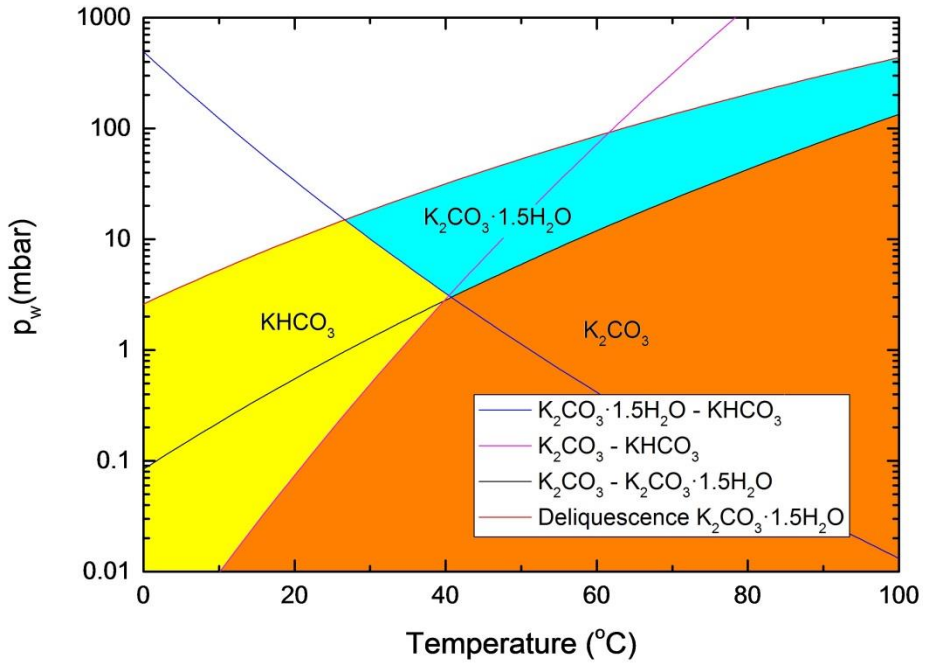

Figure 3.4. Phase diagram of the $KHCO_3$-K_2CO_3-K_2CO_3·$1.5H_2O$ system. A vapor pressure of 0.4 mbar of CO_2 is assumed.

4 Materials and methods

This chapter starts with more detailed information about the used material. Next, both TGA and DSC setups are discussed shortly. Finally, it is shown that the influence of eventual self-cooling or self-heating effects is insignificant under the used experimental conditions.

4.1 Material information

Experiments are performed with $K_2CO_3 \cdot 1.5H_2O$ crystals manufactured by Sigma Aldrich, product code: 1002118388. Particles are separated by sieving into three ranges: 50-164 μm, 300-500 μm and 710-1000 μm diameter. These three particle size ranges are named small, medium and large respectively. After sieving, the crystals are stored in a desiccator where a relative humidity of 22% is present, provided by a saturated solution of KCH_3COO. When performing TGA/DSC measurements, 6-7 mg of crystals is placed in an aluminum sample holder. Using this amount of material, a thin layer is present on the sample holder so that the eventual blocking of thermal or water vapor transport by neighboring material is minimized.

To investigate the influence of the morphology of the particles on the reaction rate, particles from a different supplier are used. These potassium carbonate crystals are manufactured by Alfa Aesar, product code: 11301578. These particles are more facetted compared to the Sigma Aldrich ones, being more granular. Particles are separated by sieving into two size ranges. Small: 50-150 μm and large: 710-1000 μm diameter.

The difference in morphology between the Sigma Aldrich and Alfa Aesar particles is made visible by means of SEM in figure 4.1. The Sigma Aldrich particles are more granular, while the Alfa Aesar particles consists of more smooth surfaces.

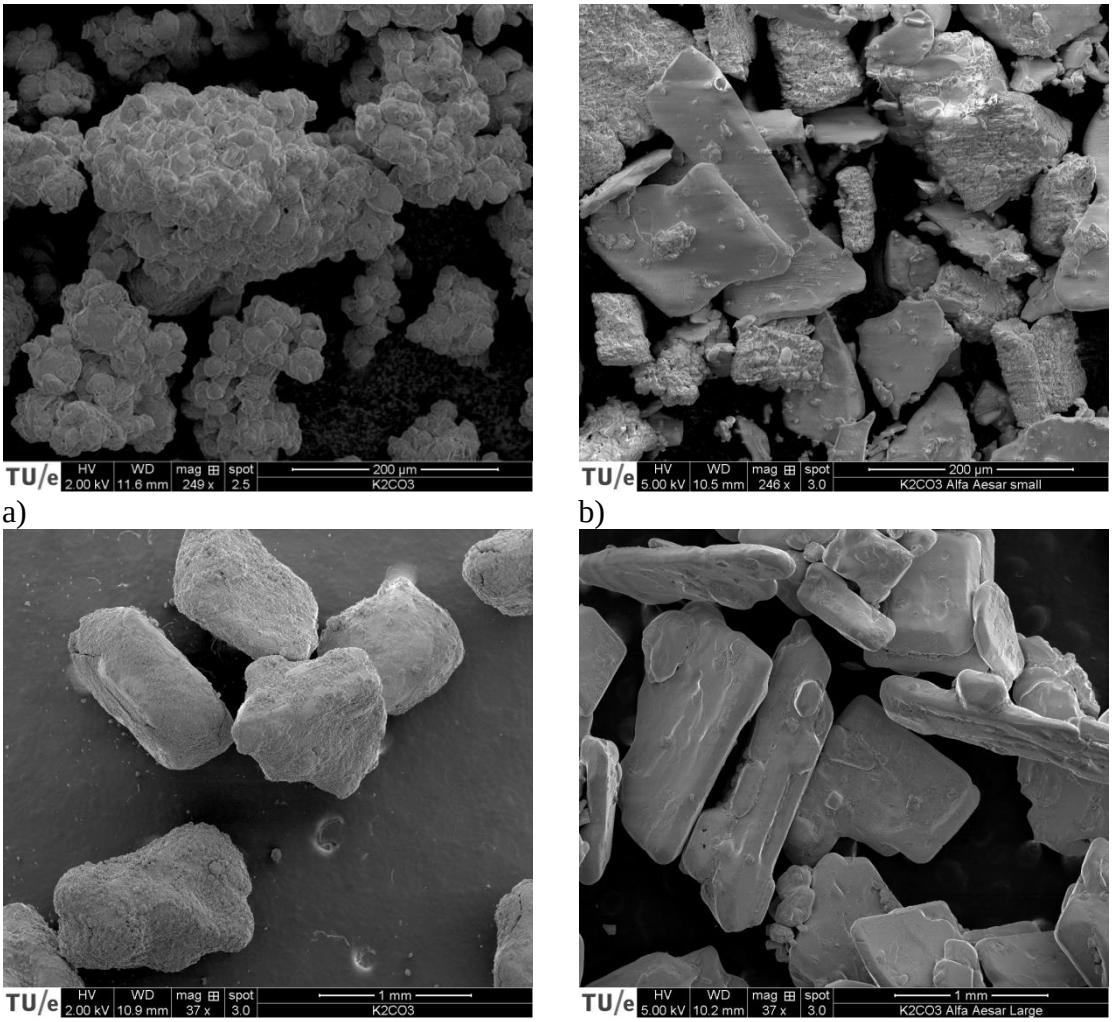

Figure 4.1. SEM pictures of potassium carbonate particles. a) small Sigma Aldrich particles. b) small Alfa Aesar particles. c) large Sigma Aldrich particles. d) large Alfa Aesar particles.

4.2 Thermogravimetric Analysis

Thermogravimetric analysis is performed using a TGA of Mettler-Toledo. The sample is placed in an aluminum crucible which is placed on the balance arm. Humid air is flown using 300 mL/min over the sample to create the wanted experimental conditions. The heating rates of 20 K/min are used to heat the sample up as quick as possible, but still controllable. In figure 4.2 a schematic is shown of the TGA setup.

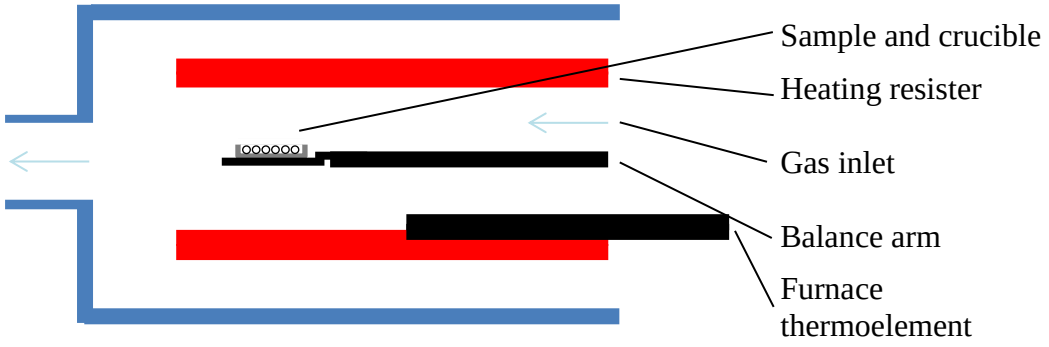

Figure 4.2. Schematic of the TGA setup.

For more information about the error approximation, choice of flow-rate, stabilization time after changing conditions and the pressure inside the TGA, one is referred to Appendix A-C.

4.3 Differential Scanning Calorimetry

The second used thermoanalytical technique is differential scanning calorimetry. A DSC measurement gives information about the heat flow as function of the time. A sample is placed under the same conditions as a reference sample throughout the experiment, see figure 4.3. Whether the reactions are exothermic or endothermic, positive or negative heat flow peaks are observed respectively, see figure 4.2. The reaction enthalpy of a phase transition can be determined by integrating the heat flow over time:

$$\Delta_r H = \int_{t_o}^{t_{final}} Q \, dt. \tag{4.1}$$

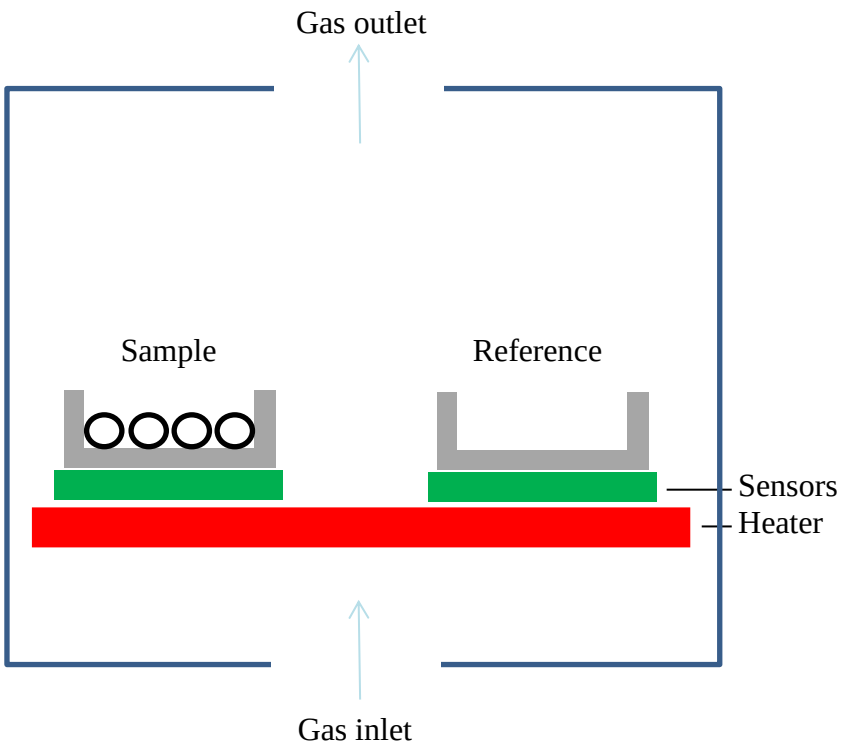

Figure 4.3. Schematic of the DSC setup.

4.4 Self-cooling & self-heating

The dehydration reaction is an endothermic process and thus requires heat to continue. When the heat supply to the reaction front is insufficient, the material may experience self-cooling and the reaction slows down. The opposite effect occurs during the hydration process and is called self-heating. When these effects are significant, the temperature is not approximately constant during the reaction process, which makes it difficult to investigate the influence of factors like the ambient water vapor pressure on the reaction rate.

Next, it will be shown that self-cooling is insignificant during the experiments performed in this project, because the contribution of thermal conduction is high enough to make up for the heat released/required by the reaction.

The temperature difference between the particle's surface and the furnace can be calculated by balancing the heat transferred to the particle from the environment with the heat required by the reaction. The main heat source is conduction: heat is transferred to the particle via the air. Newton's law of cooling gives the following expression for the heat transfer via conduction Q_c [W] [30]:

$$Q_c = 4\pi R^2 h\left(T_b - T_p\right), \tag{4.2}$$

where T_b and T_p are the temperature of the bulk furnace and the particle respectively [K] and R the particle radius [m]. The heat transfer coefficient h corresponding to air is of the order 10 W/(m^2·K) [31]. From the Stefan-Boltzmann law, the amount of heat transmitted to the particle by radiation Q_r [W] is given by [32]:

$$Q_r = 4\pi R^2 \sigma\left(T_b^4 - T_p^4\right). \tag{4.3}$$

The value of the Stefan-Boltzmann constant σ is given by $5.67 \cdot 10^{-8}$ W·m^{-2}·K^{-4}. Finally, assuming a spherical reaction front, the heat needed for reaction Q_d [W] is given by:

$$Q_d = 4\pi R^2 \Delta H_v \frac{dr}{dt}, \tag{4.4}$$

where ΔH_v is the reaction enthalpy per unit volume [J/m^3] and dr/dt the rate of reaction in units of length [m/s]. To evaluate the importance of self-cooling and self-heating, the most extreme values corresponding to the experiments are used. The highest impact was observed during the hydration in isothermal experiments at a temperature of 47.7 °C and p_w = 19.1 mbar using particles with radius 500 μm. The used rate of reaction corresponds to the maximum hydration rate during the process and is in the order of $8 \cdot 10^{-7}$ m/s.

The difference in temperature between particles surface and the ambient air is found by balancing the heat equation:

$$Q_c + Q_r = Q_d, \tag{4.5}$$

resulting in the maximum temperature difference between bulk furnace and particle: ΔT = 0.03 K.

The impact of self-heating or self-cooling is hard to measure experimentally in an accurate way. The sample is located in an aluminum pan whose temperature is measured during the experiment. However, this pan is also in contact with the ambient air and moreover, does only measure the bottom of the sample. Still, this temperature profile can be used to estimate the influence of thermal effects. The highest impact of self-heating during experiments is seen during hydration for the large particles, see figure 4.4. The temperature difference between particle and ambient air is around 0.3 °C. Compared to the calculations, the observed difference is a factor ten higher than the estimated one. This is attributed to the assumption in the calculations that the particle experiences convection all around its surface, while in reality, the particle is also surrounded by other particles which limits the influence of convective heat transport. Anyway, one concludes from the relative small temperature differences observed and estimated that the effects of self-cooling and self-heating are insignificant under the given circumstances.

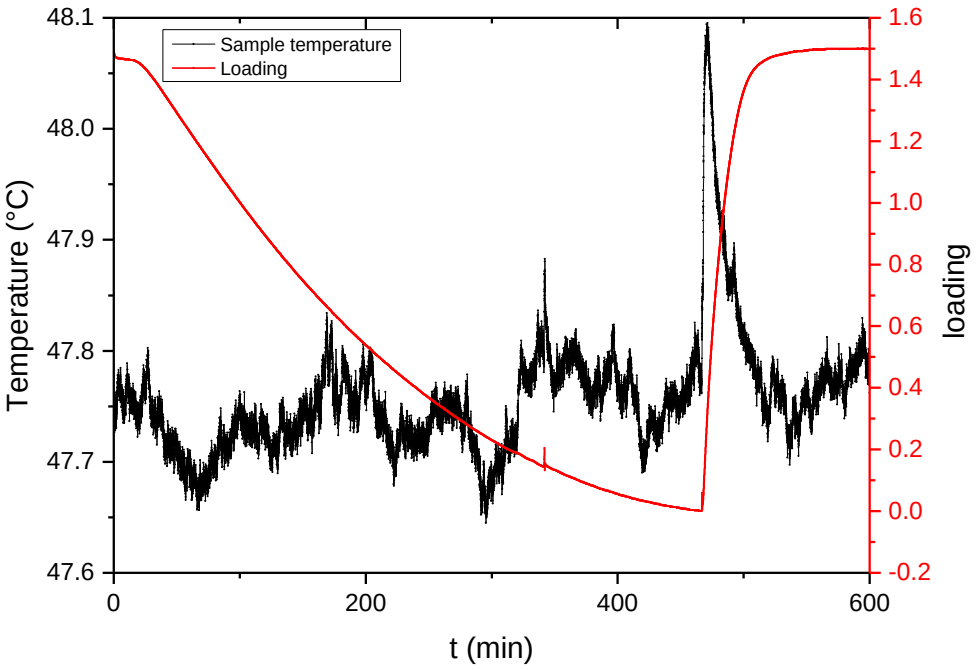

Figure 4.4. Isothermal dehydration-hydration experiment with large particles, hydration at p_w=19.1 mbar. The influence of self-cooling and self-heating is very small.

In vacuum the system will behave differently, because then, radiation is the only source/outlet of heat. This means that the influence of self-cooling and self-heating could be significantly higher.

5 Definitions & sample impurity

In this chapter, the concepts loading and reaction speed are defined by means of the sample mass. Next, the presence of impurities in potassium carbonate samples is shown and identified as potassium bicarbonate: $KHCO_3$. This is a product of hydrated potassium carbonate reacting with CO_2 from the ambient air. It is formed during storage, but not during the experiments. The mass percentage KHCO3 observed in the samples varies between 0-20%. By heating at 93 °C the $KHCO_3$ dissociates into the anhydrous material and CO_2. After proving the nature of the impurity, its consequence on the experimental results is discussed.

5.1 Defining loading and reaction speed

Before defining any reaction speeds, loading should be defined. Loading corresponds to the amount of mole water molecules per mole salt inside the hydrates lattice. The hydrated form of potassium carbonate thus has a loading of 1.5 mole H_2O per mole K_2CO_3 and its anhydrous form a loading of zero. During experiments, the loading is defined as the average loading of the sample, which is determined by the mass. When the mass of the pure hydrated or anhydrous form is known, the loading can be calculated:

$$L = \frac{m - m_{min}}{M_{H_2O}} \frac{M_{K_2CO_3}}{m_{min}}, \tag{5.1}$$

where m is the measured mass of the sample, M_{H2O} the molar mass of water, M_{K2CO3} the molar mass of potassium carbonate, and m_{min} the mass of the sample in his pure anhydrous form. The latter is related to the mass of the sample in his pure hydrated form m_{max} by:

$$m_{min} = \frac{M_{K_2CO_3}}{M_{K_2CO_3 \cdot 1.5H_2O}} m_{max}, \tag{5.2}$$

where $M_{K_2CO_3 \cdot 1.5H_2O}$ corresponds to the molar mass of hydrated potassium carbonate. In this project, the loading is calculated using the maximum mass under conditions corresponding to the hydrated form. This definition of loading is only valid when the sample consists of pure hydrated potassium carbonate. When impurities are present in the sample, the loading won't reach the expected magnitude.

The (de)hydration rate is far from constant. When evaluating any dependencies to changes in pressure or temperature, it is important to define a reaction speed. Studies from similar experiments have defined the reaction speed in different ways: averaging the reaction speed between 40% and 60% conversion [16], defining the reaction rate at 50% conversion or at its maximum rate [33]. The latter is also done using DSC experiments on $MgCl_2 \cdot 6H_2O$ by Rammelberg et al. where the reaction rate is defined at its peak power, which naturally corresponds with the maximum reaction rate [34]. In this project, the reaction speed is defined as the maximum reaction rate (loading per unit time) measured during the (de)hydration process.

5.2 $KHCO_3$ impurity

The potassium carbonate samples contain $KHCO_3$ impurities. This is a product of hydrous potassium carbonate and CO_2 from the ambient air. Firstly, it is proven that the impurity is indeed identified as potassium bicarbonate. Next, its consequence on the reaction rate is discussed.

5.2.1 Identification of the impurity

The presence of $KHCO_3$ after storing potassium carbonate samples in the presence of CO_2 is proved in this section in two different ways: by using TGA data and IR-spectroscopy.

A sample consisting of small potassium carbonate particles firstly experiences an isothermal dehydration-hydration cycle: dehydration at an ambient water vapor pressure of 0 mbar and hydration at 19.1 mbar. Next, the sample is heated for two hours at 93 °C inside the TGA setup. After heating, the temperature is lowered to 48 °C and an isothermal hydration-dehydration cycle is performed. The maximum and minimum masses corresponding to this cycle are lower in magnitude compared to the previous cycle, see figure 5.1 This indicates the possible decomposition of $KHCO_3$. To proof this hypothesis, the impurity is assumed to be $KHCO_3$ and using its molar mass the expected mass difference is calculated and compared to the measured one. More precisely, the difference between the minimum masses Δm_1 [mg] is obtained from the experiment and used to calculate the difference between the maximum masses Δm_2 [mg]. If the assumption of the impurity being $KHCO_3$ is correct, the calculated value of Δm_2 should match the value obtained from the experiment.

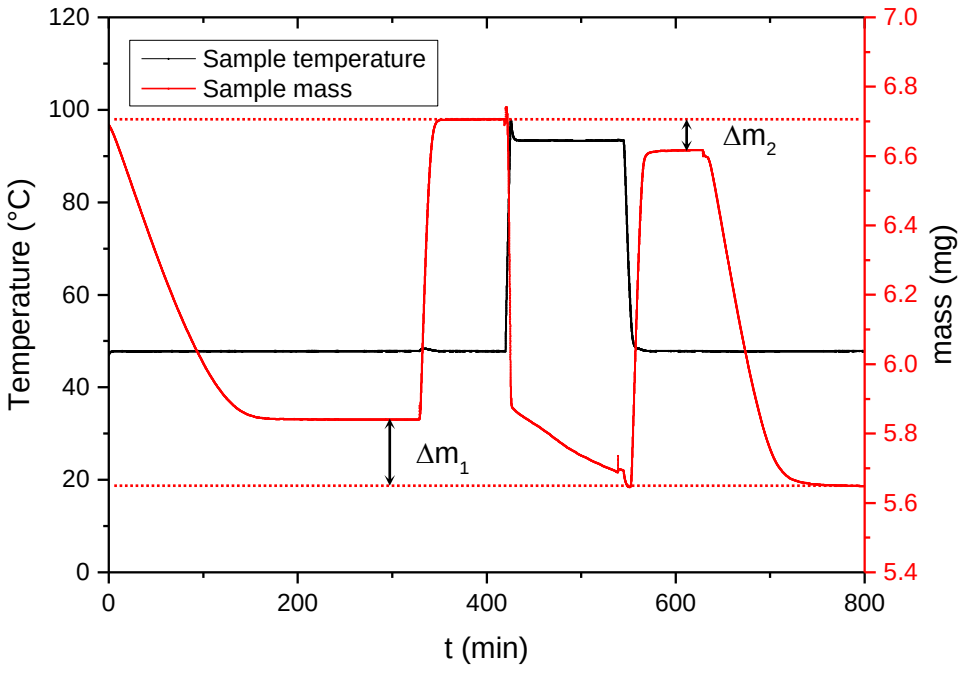

Figure 5.1. The total mass decreases after dehydrating at 93 °C, which implies impurity in the sample. Hydration at 19.1 mbar and dehydration at 0 mbar.

The mass difference corresponding to the anhydrous phases is fully determined by the amount of gas leaving the sample during decomposition of $KHCO_3$:

$$2KHCO_3(s) \leftrightharpoons K_2CO_3(s) + H_2O(g) + CO_2(g). \quad (5.3)$$

Using the corresponding molar masses one can calculate the amount of moles of H_2O and CO_2 leaving the sample, which equals the amount of K_2CO_3 formed and half the amount of $KHCO_3$ dissociated. The newly formed potassium carbonate will contribute to the mass difference Δm_2 corresponding to the hydrated phases. Thus, by using the experimentally obtained value Δm_1, the mass difference corresponding to the hydrous phases is calculated: Δm_2=0.107 mg. The mass difference corresponding to the hydrous phases obtained from figure 4.4 equals 0.089 mg. This slight difference is caused by the pan mass variation. The pan mass deviation measured using an empty pan experiment showed a mass difference of 0.01 mg during 100 minutes, see figure 5.2, which is comparable with the time interval during the heating experiment.

Above calculations based on mass differences match the assumption that the present impurity is indeed $KHCO_3$.

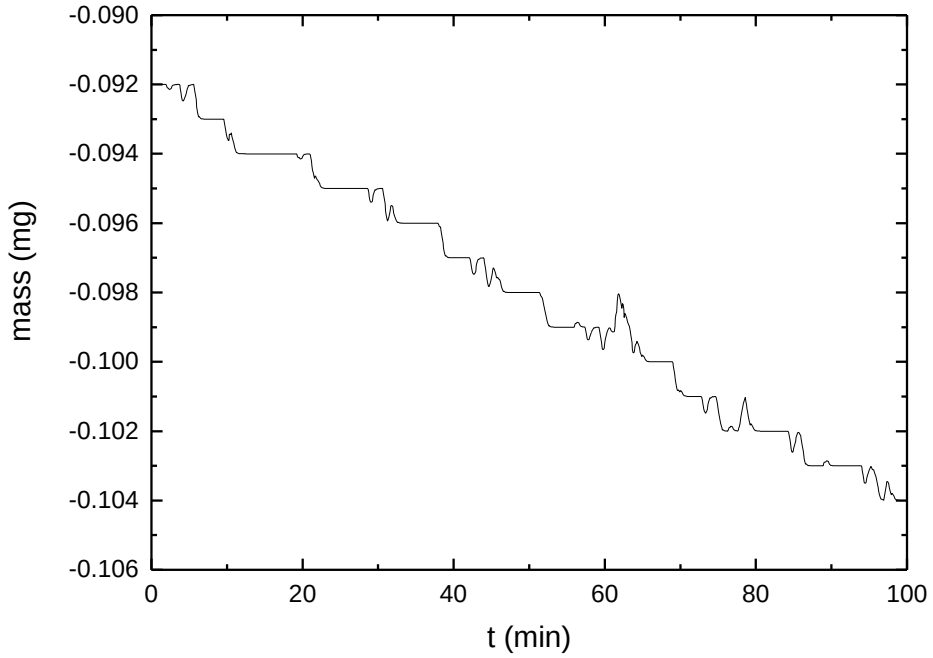

Figure 5.2. Empty pan measurement. The pan mass decreases about 0.01 mg during 100 min of heating at 93°C.

Next, IR-spectroscopy is used to check if indeed all potassium bicarbonate present is removed by heating at 93 °C [35]. Spectra of both anhydrous potassium carbonate and potassium bicarbonate are obtained from literature [36] (black line and red line, see figure 5.3). The $KHCO_3$ spectrum shows a peak at 1631 cm^{-1}, while this peak is absent for the pure K_2CO_3. The blue line corresponding to hydrous K_2CO_3 used in experiments, before any cycling, shows a similar peak. As a check, potassium bicarbonate is measured (pink line), which is similar to the literature spectrum. The green and dark blue line correspond to potassium carbonate used in experiments after heating it for a few hours at 93 °C. The peak at 1631 cm^{-1} is now absent. The purple line corresponds to the same potassium carbonate sample after adding a droplet of water: pure hydrated potassium carbonate.

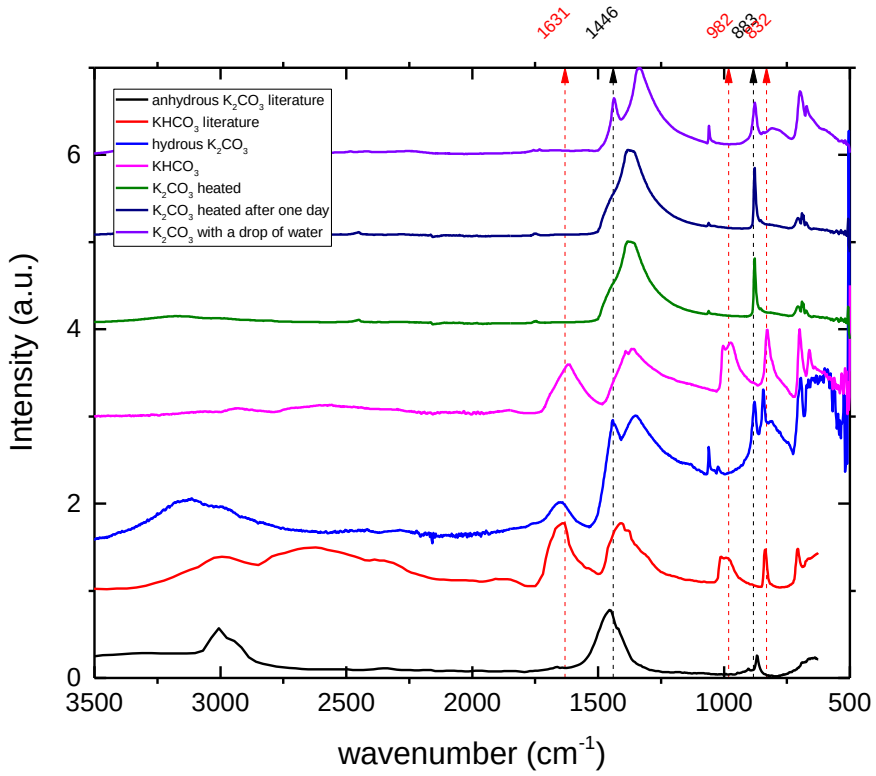

Figure 5.3. IR-spectra of K_2CO_3 and $KHCO_3$ show the presence of $KHCO_3$ in the initial samples. Heating it at 93 °C removes it entirely.

5.2.2 Consequences of the impurity

In previous sections the presence of $KHCO_3$ in the sample is proven, which makes the samples partially impure. During most experiments the samples are initially dehydrated at a temperature of 93 °C and thus the potassium bicarbonate decomposes. However, also isothermal experiments are performed at 48 °C. $KHCO_3$ is stable at this temperature and thus the sample mass has to be corrected with respect to the amount of impurity present: the amount of potassium bicarbonate present in the sample is calculated and subtracted from the sample mass. In this way, reaction rates corresponding to differently impure samples can be compared. However, this is only valid if two conditions are met.

Firstly, the amount of impurity present in the sample should remain the same during the experiment. This is the case, because the minimum and maximum masses remain the same during the experiment, see figure 5.4. This means that no potassium bicarbonate is formed nor dissociated during the experiment.

Secondly, the amount of impurity in the sample should not have an impact on the reaction rate. The sample corresponding to the measurement visible in figure 4.4 has a mass percentage $KHCO_3$ of 21% before heating, the maximum hydration rate is measured to be (0.145±0.002) mol H_2O per mole K_2CO_3 per minute. After heating for two hours, the mass percentage KHCO3 is decreased to 11% and a maximum hydration rate of (0.147±0.002) mol H_2O per mole K_2CO_3 per minute is observed. The difference in hydration rates is within the margin of error so one can conclude that the amount of $KHCO_3$ present within the sample does not impact the reaction rate significantly.

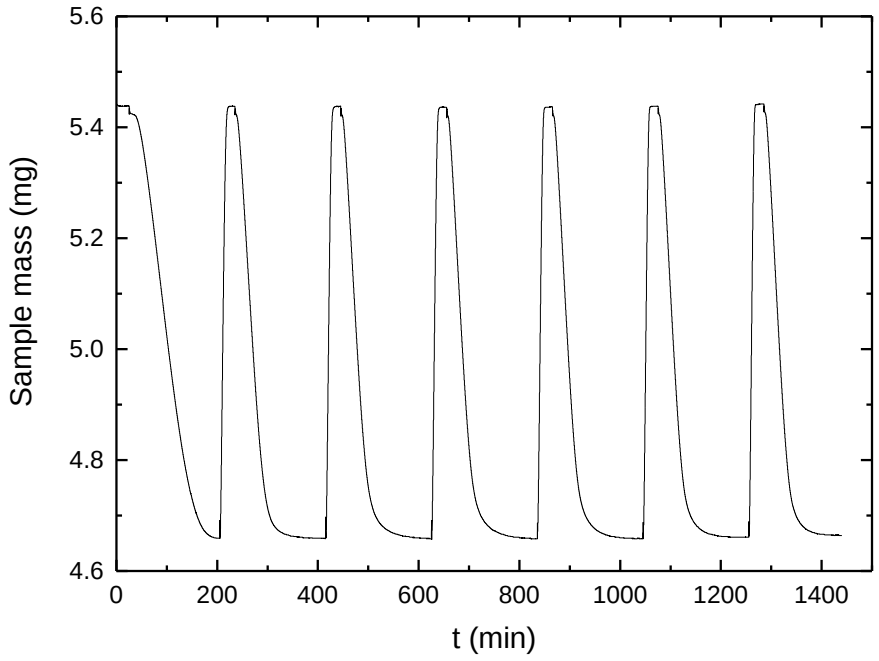

Figure 5.4. TGA measurements of consecutive cycles of small particles, uncorrected. Isothermal at 48 °C. Hydration at 19.1 mbar and dehydration at 0 mbar.

6 Hydration-dehydration cycling

The behavior of reaction rate during dehydration-rehydration cycling of potassium carbonate is discussed in this chapter. Firstly, hydration and dehydration rates are investigated using isothermal TGA experiments and different particle sizes and morphology. These experiments are repeated using the DSC technique. Next, reaction rates as function of the number of experienced cycles are investigated using temperature cycling TGA experiments at a constant water vapor pressure. The reaction speed turns out to increase for subsequent cycles until a certain maximum is achieved due to morphologic changes in the material.

6.1 Isothermal cycling – loading

Isothermal dehydration-rehydration cycles are performed at a temperature of 48 °C using three different particle sizes in the TGA setup. Dehydration is done with dry air and the sample experiences a vapor pressure of 19.1 mbar during hydration. Experiments are performed using both Sigma Aldrich and Alfa Aesar particles. Dehydration-hydration cycles of small, medium and large potassium carbonate particles provided by Sigma Aldrich are shown in figure 6.1. The dotted lines show the water vapor pressure profile. The dehydration time given in the first cycle corresponding to the medium and large particles is longer compared to subsequent ones.

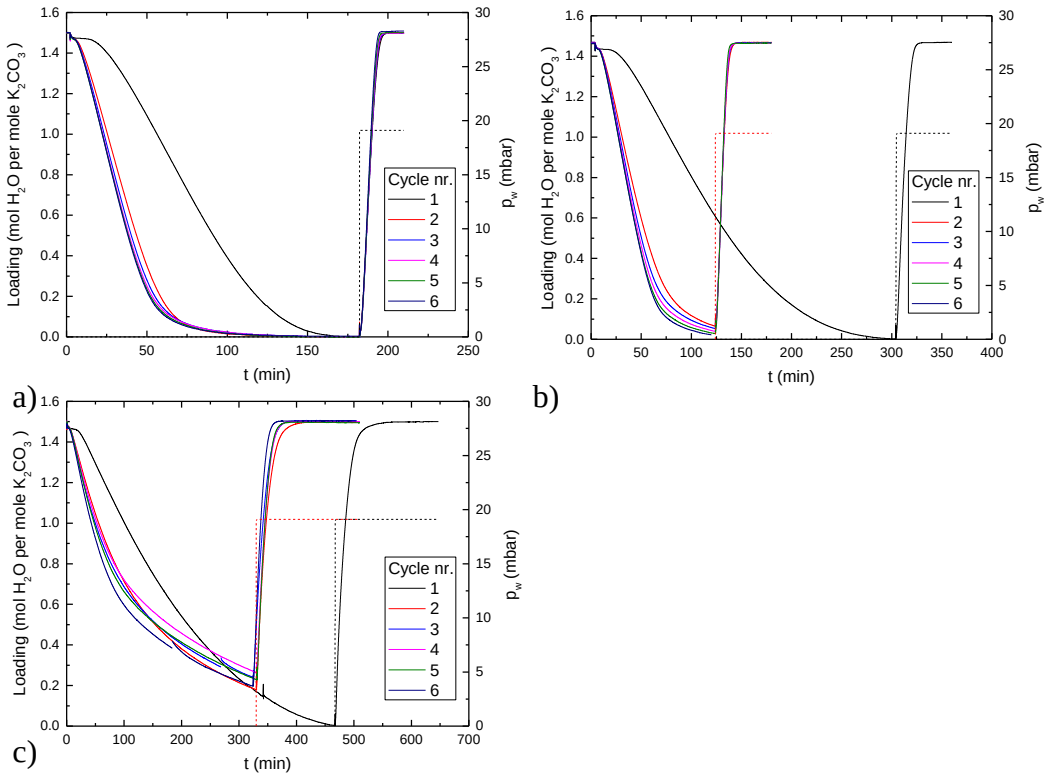

Figure 6.1. TGA measurements of consecutive cycles potassium carbonate particles, Sigma Aldrich. Isothermal at 48 °C. Hydration at 19.1 mbar and dehydration at 0 mbar. a: small particles (50-164 µm diameter), mass percentage $KHCO_3$ in the sample: 14.5%. b: medium particles (300-500 µm diameter), mass percentage $KHCO_3$ in the sample: 19.6%. c: large particles (710-1000 µm diameter), mass percentage $KHCO_3$ in the sample: 6.0%.

Isothermal dehydration-hydration cycles of small and large potassium carbonate particles provided by Alfa Aesar are shown in figure 6.2. These particles are less granular and have more equal surfaces compared to the Sigma Aldrich ones.

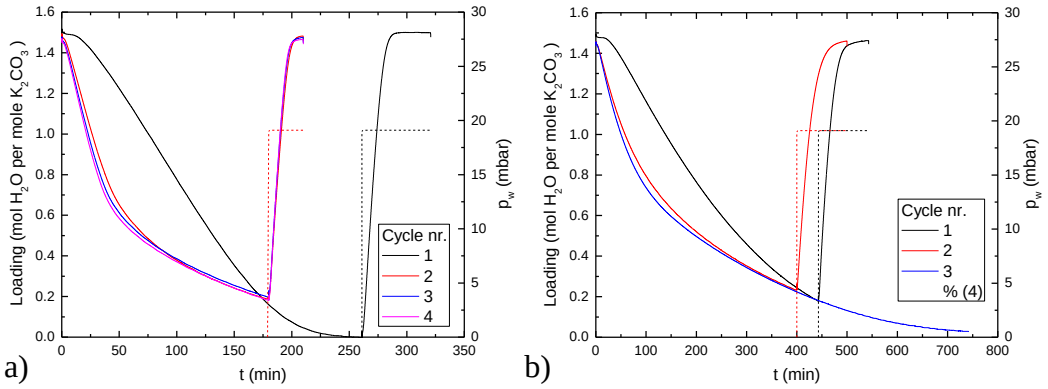

Figure 6.2 TGA measurements of consecutive cycles of potassium carbonate particles, Alfa Aesar. Isothermal at 48 °C. Hydration at 19.1 mbar and dehydration at 0 mbar. a: small particles (50-150 µm diameter), mass percentage $KHCO_3$ in the sample: 15.5%. b: large particles (710-1000 µm diameter), mass percentage $KHCO_3$ in the sample < 1%.

These isothermal experiments lead to the following insights: firstly, the reaction rate increases as the number of performed cycles increases and eventually becomes stable. Interestingly, the initial dehydration process takes very long compared to the subsequent ones. In figure 6.3 the hydration and dehydration rates corresponding to the different particles are plotted versus the number of experienced cycles. The error caused by eventual overestimating the amount of impurity corresponding to the large particles is insignificant compared to the total error.

The hydration rates corresponding to the Alfa Aesar particles are substantially lower compared to the Sigma Aldrich particles. This is discussed in more detail in section 6.3.3. This difference is not observed for the dehydration rate.

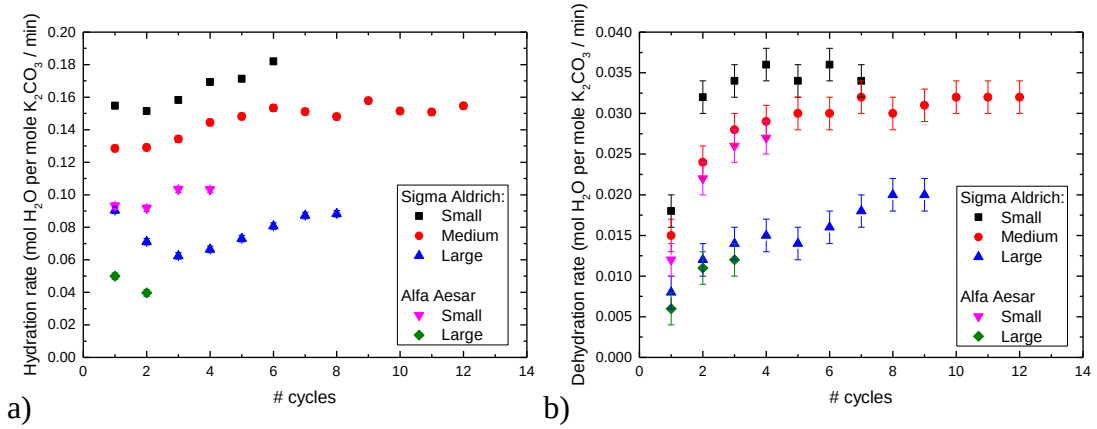

Figure 6.3. Reaction rate as function of the number of experienced cycles. Isothermal at 48 °C. Hydration at 19.1 mbar and dehydration at 0 mbar. a: hydration rate. b: dehydration rate.

6.2 Isothermal Cycling – heat

To get more insight into the heat generation and absorption of K_2CO_3 during cyclic hydration-dehydration, isothermal measurements are performed using the DSC technique. The resulting signal corresponds with the heat given or absorbed by the sample as a function of time. The endothermic dehydration step is a negative peak, while the exothermic hydration step is visualized with a positive peak. The reaction enthalpy is given by the integral over such a peak. The total sum of both enthalpies should be, in theory, equal to zero. By dividing the integral till a certain time by the total integral, a conversion curve can be made. The conversion X is given by the following relationship:

$$1 - X = \frac{\int_{t_0}^{t} q \, dt}{\int_{t_0}^{\infty} q \, dt}, \tag{6.1}$$

where t_0 is the start of the peak, t the wanted time and the heat flow q [W] corresponds to the magnitude of the signal given by the DSC. For a perfectly pure sample, loading-time curves can be made by multiplying the conversion curve by 1.5. However, due to fact that impurities are present in the isothermal cycling experiments, the choice is made to express the reaction rate in units of mW/mg. Here the mass is defined by the initial mass of the sample: a combination of potassium sesquihydrated and potassium bicarbonate.

Firstly, the change in rate during cycling for different particle sizes is investigated. Next, it is checked whether the particle has to “restabilize” when the temperature changes..

Different particle sizes

During isothermal experiments the temperature is set constant at 50°C and the vapor pressure is varied from 22.5 mbar to 0 mbar to enforce hydration and dehydration respectively. The results of DSC measurements on different particle size fractions are shown in figure 6.4. Just like observed in the TGA measurements, the difference between the first step compared to the subsequent ones is significant.

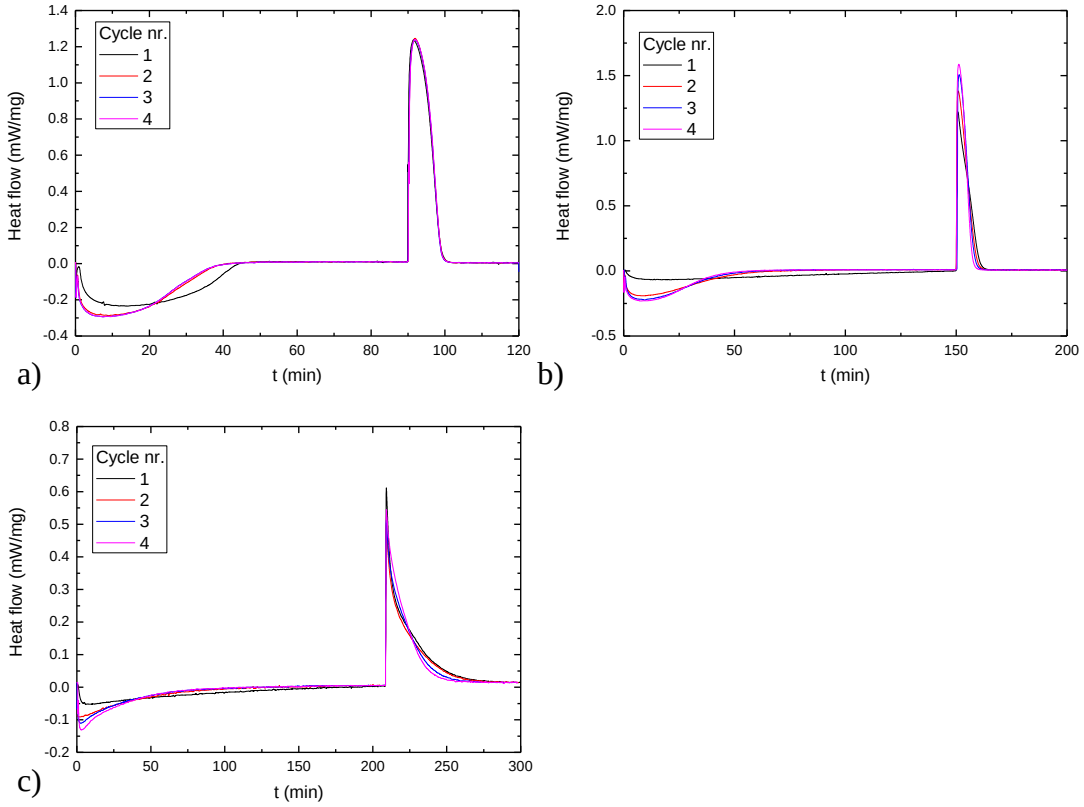

Figure 6.4. DSC measurements of consecutive cycles of potassium carbonate particles, Sigma Aldrich. Isothermal at 50°C. Hydration at 22.5 mbar and dehydration at 0 mbar. a: small particles (50-164 µm diameter). b: medium particles (300-500 µm diameter). c: large particles (710-1000 µm diameter).

Next, the maximum signals are normalized over the initial mass and plotted vs the number of experienced cycles, see figure 6.5. The DSC experiments show similar behavior compared to the TGA experiments The first hydration cycles corresponding to the medium particles are left out, because during this time the cooling in the lab was broken. Therefore, the used airflow was more humid compared to the other samples. After 8 cycles, the temperature is normal again and the ambient water vapor pressure is 22.5 mbar.

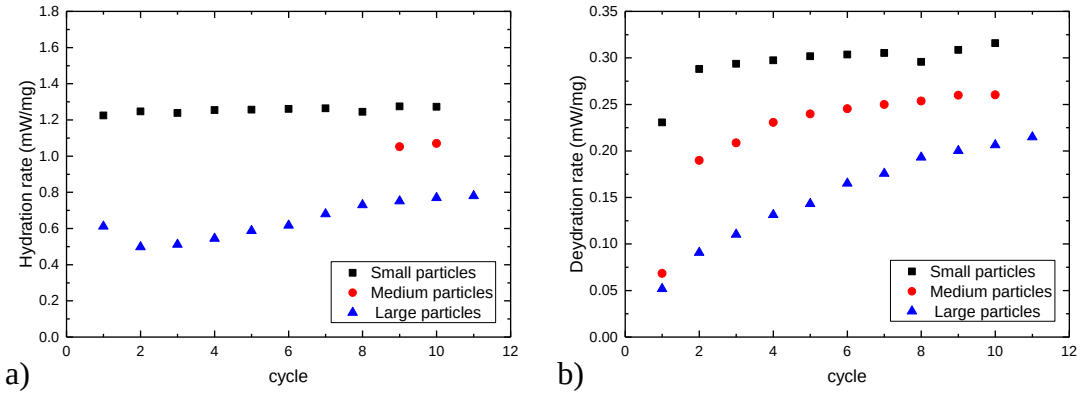

Figure 6.5. Reaction rate as function of the number of experienced cycles. Isothermal at 50°C. Hydration at 19.1 mbar and dehydration at 0 mbar. a: hydration rate. b: dehydration rate.

Stability check

According to earlier results, the rate of hydration/dehydration reaches a steady state after a number of cycles. This indicates a structural change in the material. The material eventually has an optimum structure so the dehydration-hydration processes are speed up. This hypothesis is discussed in more detail in section 6.4. To check if this final structure is different under other environmental circumstances the following experiment is performed. A sample, which is initially stabilized using isothermal cycling at 60 °C, undergoes cycling at 50 °C. The results are shown in figure 6.6.

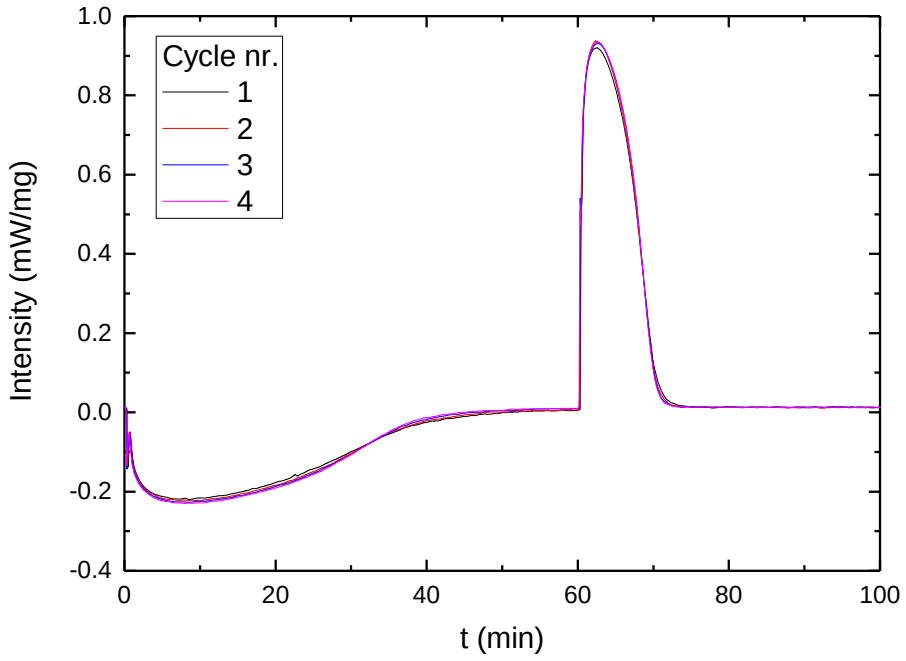

Figure 6.6. Medium K_2CO_3 particles (300-500 µm diameter), Sigma Aldrich, initially stabilized by isothermal cycling at 60°C, are still stable when cycling at 50°C.

The difference in signal between the consequent cycles is minimal compared to the difference of the first cycles of a not stabilized sample. One can conclude that the sample, which was stabilized at 60 °C, is still stable at a lower temperature of 50 °C. This means that, for further experiments where the stabilized material is of interest, it is allowed to stabilize it in using fastest way. Even if the experiment itself is under different conditions.

6.3 Temperature cycling

By increasing and decreasing the temperature for the dehydration and hydration processes respectively, the total experimental time is shortened and thus more cycles can be measured within the same time span. Initially the sample is dehydrated for 120 minutes. One single cycle consists of two different parts: dehydration at 93 °C for 40 minutes followed by rehydration of the sample at 26 °C for 80 minutes. The pressure during the experiment remains constant at 8.9 mbar.

The temperature inside TGA needs time to stabilize, especially the cooling process needs some time. The difference between the reference temperature, which is the temperature imposed by the software, and the actual temperature of the sample itself is shown in figure 6.7. The temperature needs around 25 minutes to reach a constant temperature of 26 °C, during this time the hydration process is already started. From the figure one notices that the sample temperature do not match the imposed temperatures. This is caused by the air blown into the TGA, which is used to impose a certain vapor pressure. The air cools down the sample in the TGA when measuring at high temperatures. The temperatures corresponding the experiments are the sample temperature measured by the setup.

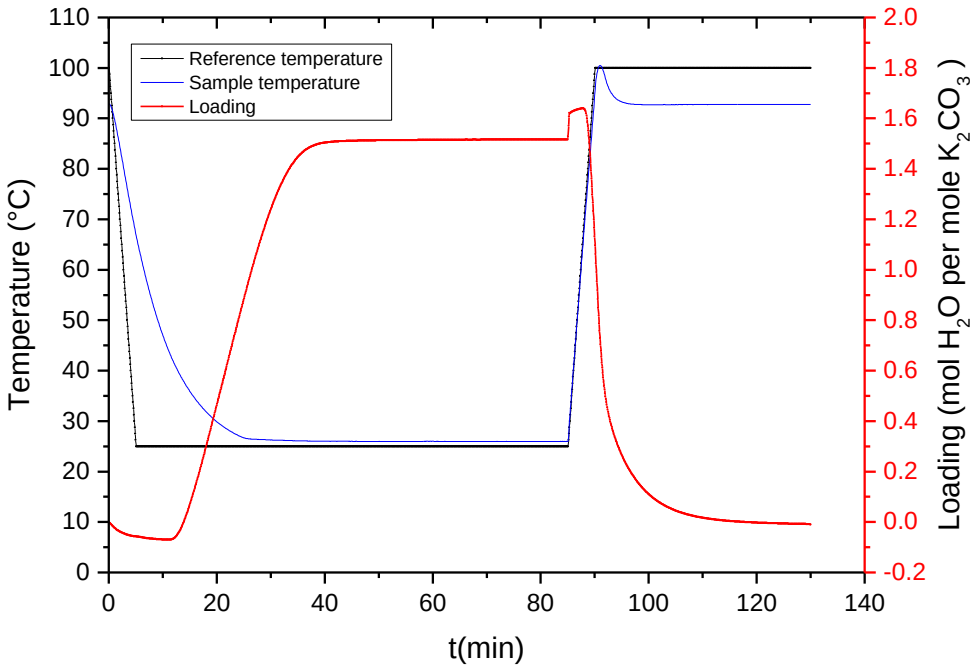

Figure 6.7. Used temperature profile (blue) and the temperature experienced by the sample (red), Sigma Aldrich. Dehydration at 93 °C and hydration at 26 °C. Ambient water vapor pressure of 8.9 mbar.

At the start of a cycle, the material is dehydrated and the temperature is decreasing. The initial decrease of loading is a direct cause by this temperature decrease, it is also visible when doing a reference measurement using an empty pan. When the temperature is low enough, the sample starts hydrating. The small peak at the end of the hydration process denotes the moment the temperature starts increasing to 93 °C. Also this peak is visible during the reference measurement and thus has no significance for the experiment. Due to the high temperature the sample dehydrates and eventually reaches a loading around zero.

The cyclic behavior corresponding to the different particle fractions of Sigma Aldrich particles are shown in figure 6.8. The experimental data of the Alfa Aesar particles is shown in figure 6.9.

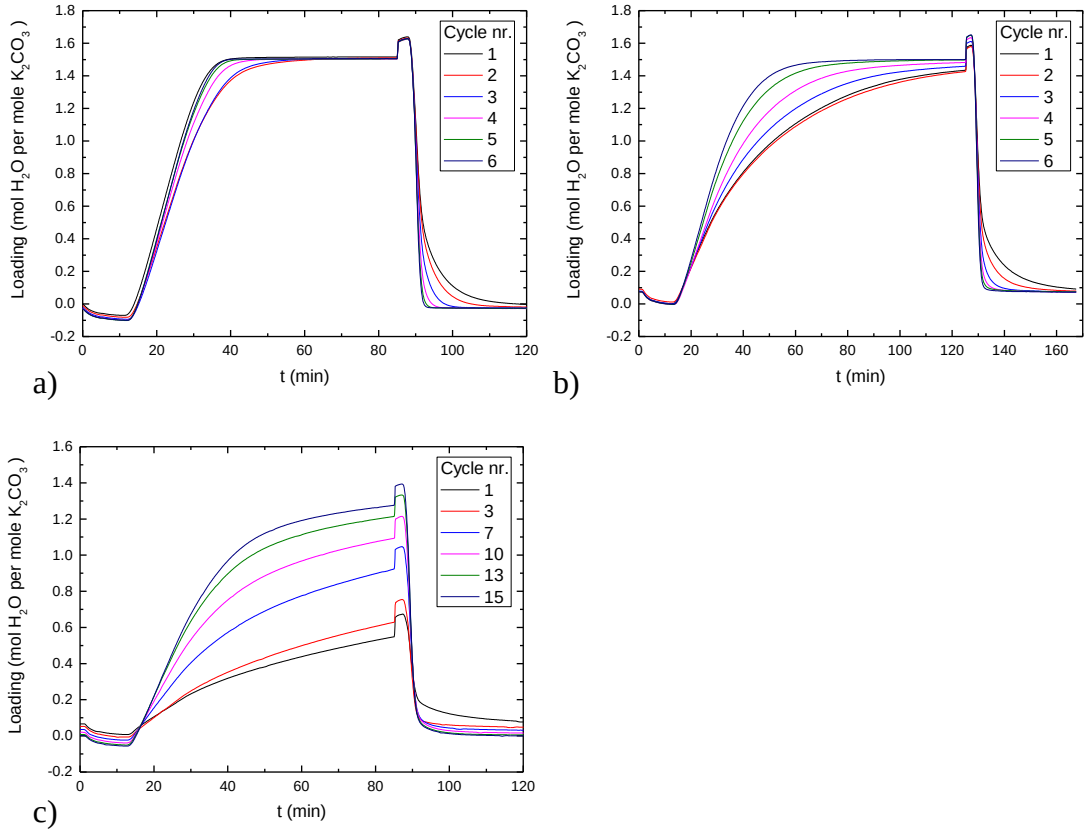

Figure 6.8. TGA measurements of consecutive cycles of potassium carbonate particles, Sigma Aldrich. Dehydration at 93 °C and hydration at 26 °C. Ambient water vapor pressure of 8.9 mbar. a: small particles (50-164 µm diameter). b: medium particles (300-500 µm diameter). c: large particles (710-1000 µm diameter).

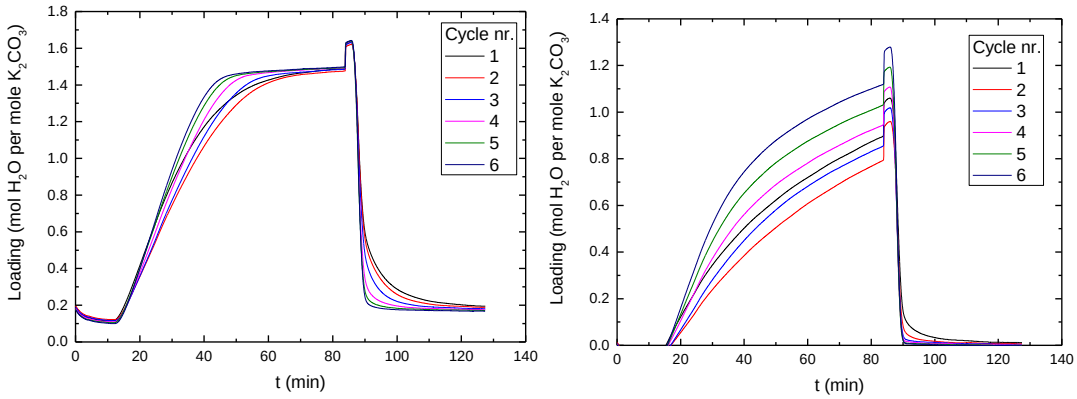

Figure 6.9. TGA measurements of consecutive cycles of potassium carbonate particles, Alfa Aesar. Dehydration at 93 °C and hydration at 26 °C. Ambient water vapor pressure of 8.9 mbar. a: small particles (50-150 µm diameter). b: large particles (710-1000 µm diameter).

Subsequent cycles turn out to reach their final states faster compared to the initial ones, this is observed for both the hydration phase and dehydration phase. The maximum reaction speeds as a function of the number of experienced cycles are plotted in figures 6.10. The reaction rate increases for both cases asymptotically, the same behavior is observed for different particle sizes. The number of cycles needed to reach the maximum reaction rate is higher for larger particles. These observations match the results from the isothermal experiments.

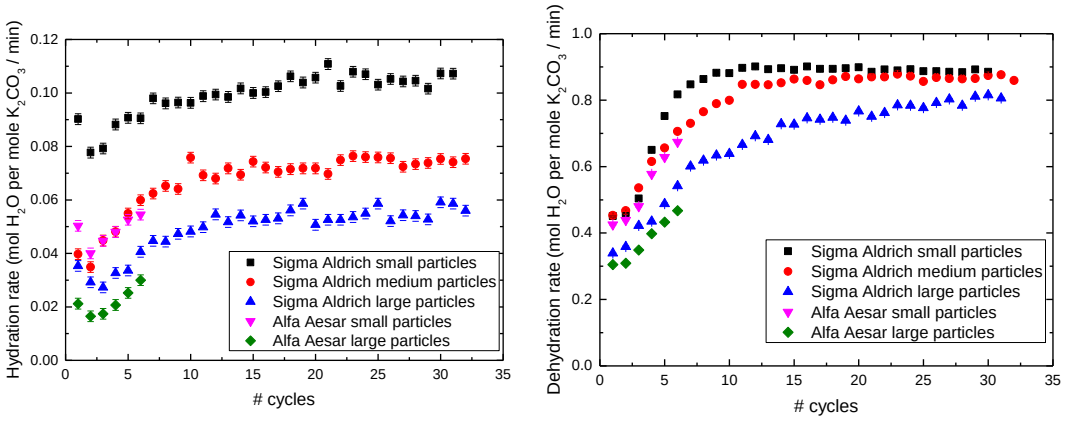

Figure 6.10. Reaction rate as function of the number of experienced cycles. Dehydration at 93 °C and hydration at 26 °C. Ambient water vapor pressure of 8.9 mbar. a: hydration rate. b: dehydration rate.

The same behavior is observed for potassium carbonate particles for both suppliers. However, the hydration rate as function of the number of experienced cycles of the small Alfa Aesar is low compared to the Sigma Aldrich ones, see figure 6.10a. This difference in magnitude is also observed during isothermal experiments, see figure 6.3a. This is explainable by taking the difference in morphology in mind. The Alfa Aesar particles are less granular and have more equal surfaces compared to the Sigma Aldrich ones, which indicates a lower contact surface with the ambient water vapor.

6.4 Discussion

In the previous sections the reaction rate of both the hydration and dehydration processes are investigated using TGA and DSC experiments. The reaction rates turned out to initially increase due to cycling and eventually reach a steady state. When hydrating, the particle and its grains increase in size due to the intake of water. After the subsequent dehydration the grains get back to their old size, but the distance between the grains may have increased. Due to these larger pores the water transport is improved and the reaction rate increases. A confirmation of this hypothesis is that the sample after experiments is increased in size compared to the initial sample, even though it is in the same state. In figure 6.11, a schematic is shown explaining the process. The process described above is observed by Mackaij using SEM during cycling experiments, see figure 6.12 [37].

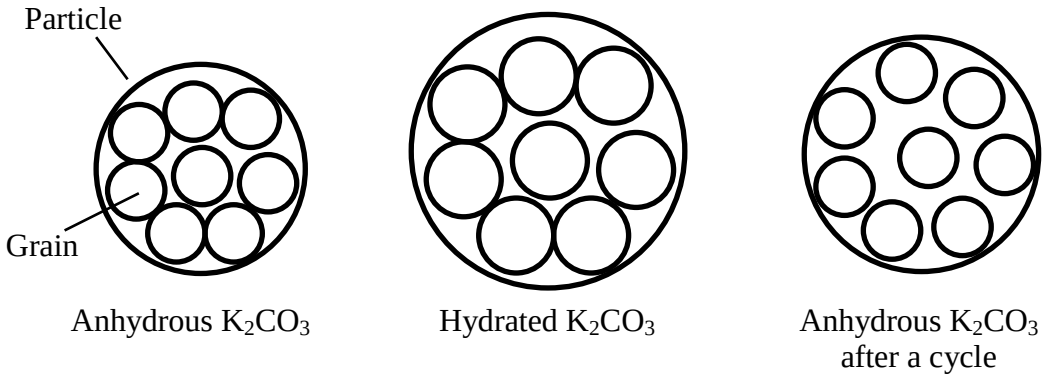

Figure 6.11. Schematic of the particle morphologic changes during a hydration-dehydration cycle.

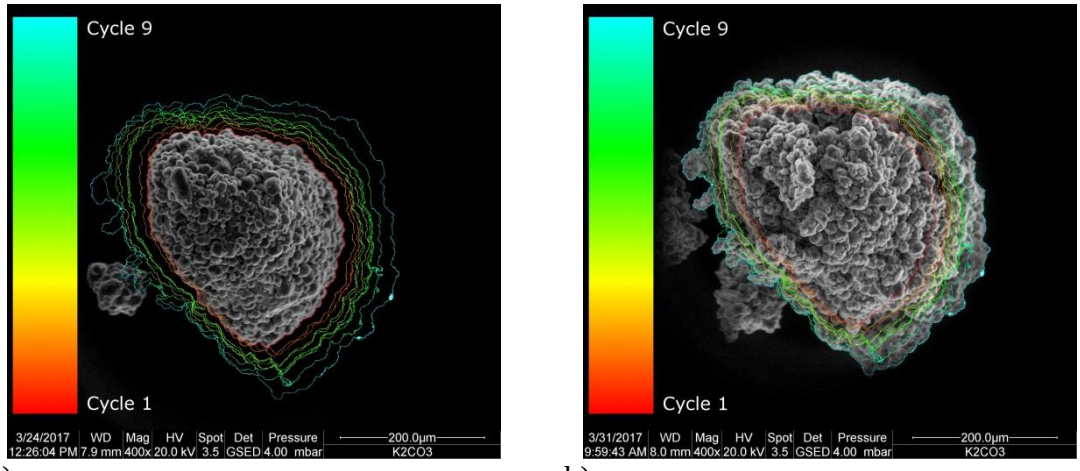

a) b)

Figure 6.12. SEM pictures show an increase of particle volume due to cycling [37]. a: anhydrous potassium carbonate in the first cycle. b: anhydrous potassium carbonate in the 9th cycle.

In order to distinguish any trends the relative increase of rate is summarized for the different methods in figure 6.13. The relative rate is defined as the reaction rate corresponding to the final measured cycle divided over the initial reaction rate.

The relative hydration rates corresponding to the isothermal TGA experiments have a value close to 1, meaning that there is no significant acceleration of the reaction process. This is the case for all three particle size ranges. The relative hydration rates obtained by the DSC experiments show the same. However, the temperature cycling experiments show relative hydration rates higher than 1 for the medium and large particles, so no clear relationship between particle size and the acceleration of the hydration process by cycling is observed.

The dehydration experiments show that the relative dehydration rate is dependent of particle size: the rate corresponding to the large particles increases relatively more compared to smaller ones. The magnitude of the relative dehydration rates corresponding to the isothermal TGA experiments are similar to the values obtained from the TGA temperature cycling experiments. However, the relative dehydration rates corresponding to the isothermal DSC experiments are almost twice as high. It is difficult to give a physical explanation for this, because the samples used in the DSC experiments contain an unknown amount of impurity, causing the absolute values of the reaction rates to be possibly inaccurate.

The relative dehydration rates obtained from the isothermal TGA experiments are higher in magnitude compared to the relative hydration rates. The results from the other methods match this behavior. This means that the dehydration process is relative more favored by cycling compared to the hydration process.

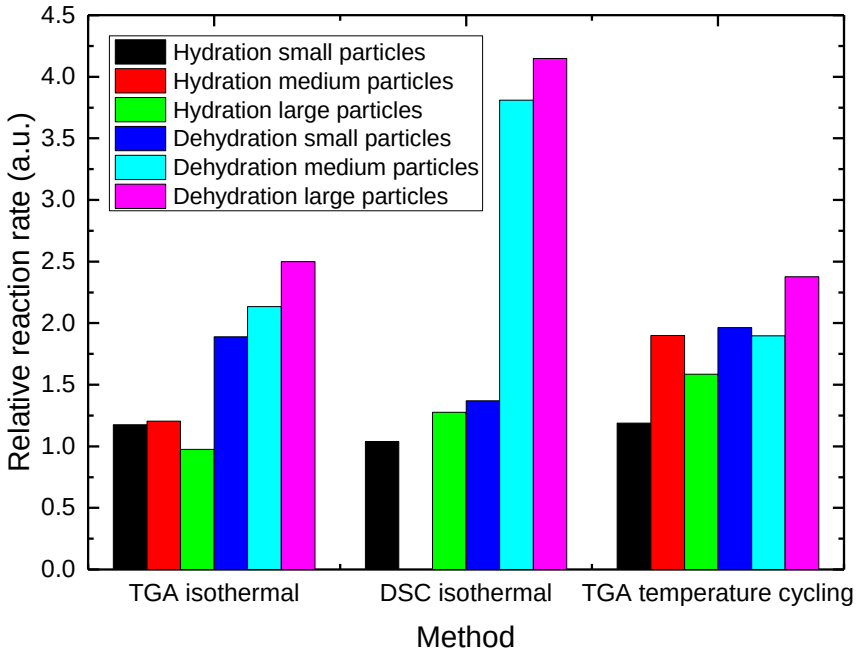

Figure 6.13. Overview of the relative increase of rate of the cycling experiments with Sigma Aldrich particles.

7 Water vapor pressure dependency

In this chapter, the water vapor dependency of the reaction rate is investigated. Firstly, experimental results from hydration experiments at different temperatures are shown and evaluated. Secondly, the water vapor dependency of the dehydration process is investigated.

To be sure that no effects caused by cycling will be observed during the experiments, stable samples are used. The potassium carbonate samples have undergone over 50 dehydration-hydration cycles and no differences between subsequent cycles was present anymore. The cycling is performed in the DSC setup, where hydration occurred at 25 °C with a vapor pressure of 10 mbar. The dehydration process happened at 100 °C using the same water vapor pressure.

7.1 Hydration

Hydration experiments are performed as following: the sample is dehydrated using only a dry air flow and a temperature of 93 °C. Next, the temperature is lowered until the desired sample temperature is reached. Then, the water vapor pressure is increased to a certain value so the hydration process occurs. These proceedings are repeated for varying water vapor pressures. To exclude the impact of any eventual effects caused the history of the sample, the subsequent experiments are first performed by increasing pressure and also repeated by decreasing pressures. The measurements are performed at three different temperatures: 26 °C, 39 °C and 48 °C. The results can be plotted as a function of the vapor pressure, as shown in figure 7.1. The same measurement points are also plotted as function of p_w/p_{eq}, see figure 7.2.

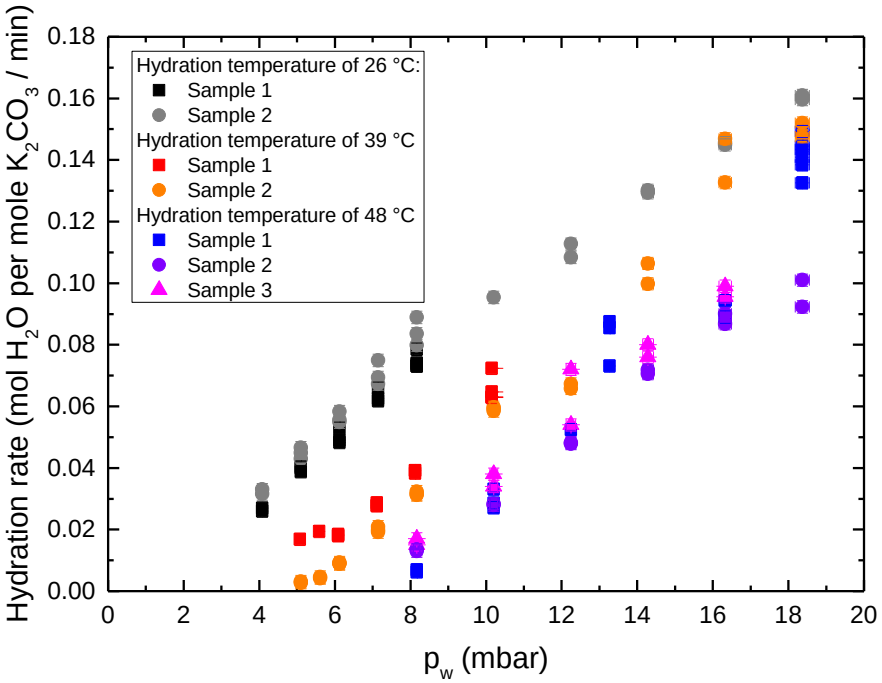

Figure 7.1. Hydration rate as function of the water vapor pressure at three different temperatures.

From figure 7.1 one concludes that the rates remain more or less the same for different samples, which means that the reproducibility of the experiment is good. The second observation is the need of a certain overpressure to start the reaction. At 26 °C, no reaction was observed for pressures lower than 5 mbar during the given time while the present water vapor pressure is higher than the equilibrium pressure. And when reaction occurs, the reaction rate starts relatively high, not like measured at higher temperatures. When started, the reaction rate seems to be more or less linear dependent to the vapor pressure.

Rehydration experiments are also performed by Stanish and Perlmutter [16]. Rates were found to be very slow at pressures close to the equilibrium value $p_w/p_{eq} < 1.5$ and become linear for $p_w/p_{eq} > 3$. Another observation done by Stanish and Perlmutter is that the samples that were dehydrated more rapidly (at higher temperature and/or lower pressure) were subsequently found to rehydrate more rapidly as well. This behavior is not observed during experiments: the measurements at 48 °C using the first sample were performed isothermally, while the rest dehydrates at a temperature of 93 °C. According to Stanish and Perlmutter, the second sample at 48 °C, which has dehydrated more rapidly compared to the first sample, should have a higher hydration rate. However, this difference is not observed.

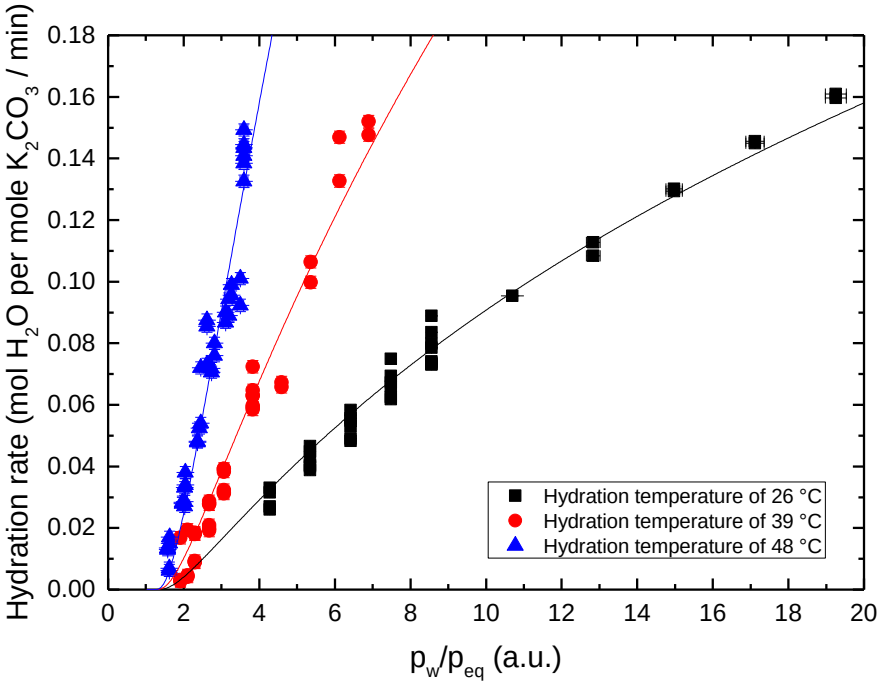

Figure 7.2. Hydration rate as function of the ratio of water vapor pressure and the equilibrium pressure at three different temperatures. The data is fitted using eq. 6.25.

From a thermodynamic point of view, one would expect the material to hydrate at all water vapor pressures higher than the equilibrium water vapor pressure. However, as shown in figure 7.2, the hydration processes corresponding to hydration temperatures of 39 °C and 48 °C do not start till $p_w/p_{eq} \approx 1.5$. The hydration process corresponding to a temperature of 26 °C even needs a higher water vapor pressure. The lack of any hydration implies that the process is limited by the nucleation step: no, or too few nuclei corresponding to the hydrous phase are formed during the given time. The classical nucleation theory as described in section 2.3 shows that the nucleation rate

remains approximately zero and then increases rapidly after a certain water vapor pressure is reached. This exact point is difficult to predict, because it is dependent of the surface energy $\gamma_{m,n}$, whose magnitude is not known.

Interestingly, the experimental hydration data shows similar behavior as found for the nucleation rate using the theory. For this reason, the hydration data in figure 7.2 is fitted using the classical nucleation model as described in section 2.3, resulting in the fit parameter: $\gamma_{m,n} = (0.0041 \pm 0.002)$ J/m^2.

The nucleation mechanism of solid-solid phase transitions is investigated using microscopy by Peng et al. [38]. They observed a two-step nucleation pathway: an intermediate liquid state is formed, then solid nuclei are formed from this intermediate state. Following this reasoning, one expects to find a value of $\gamma_{m,n}$ in the order of 0.3 J/m^2, which corresponds to the surface tension of NaCl [22]. The obtained value of $\gamma_{m,n}$ is a factor 100 smaller than the surface energy of NaCl found in literature. The difference in magnitude observed can be explained by the fact that the $\gamma_{m,n}$ in the model is a microscopic quantity describing the surface energy of a nucleus, while usually the surface energy describes a macroscopic quantity. However, it could also be the case that the experimental data cannot be described using the classical nucleation model: this theory describes only the nucleation process; any propagation effects are ignored.

Finally, Arrhenius analysis is performed on the experimental data as described in section 2.5. For this purpose, $f(p_w/p_{eq})$ is approximated to be linear, resulting in an activation energy E_a of (98 ± 2) kJ/mol K_2CO_3. The corresponding fits are shown in figure 7.3. One notices that the activation energy is similar to the obtained hydration enthalpy ΔH of (97.1 ± 2) kJ/mol K_2CO_3. It is also comparable with the activation energy for $K_2CO_3 \cdot 1.5H_2O$ dehydration in vacuum of approximately 91 kJ/mol K_2CO_3, found by Stanish and Perlmutter [15].

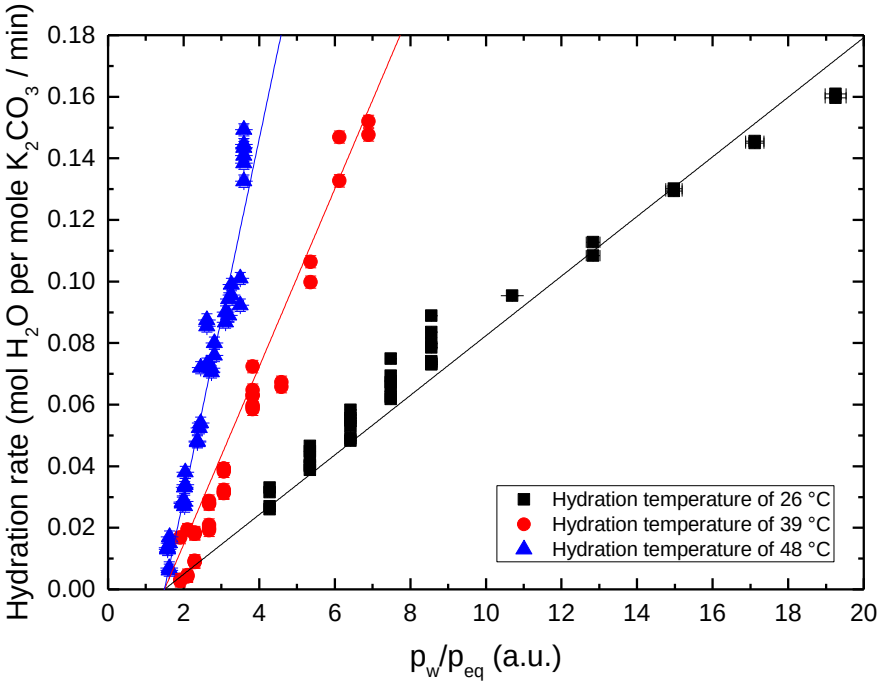

Figure 7.3. Arrhenius analysis performed on the hydration rate as function of the ratio of water vapor pressure and the equilibrium pressure at three different temperatures, E_a = (98 ± 2) kJ/mol K_2CO_3.

A master curve corresponding to the hydration process is made by dividing the hydration rate by the temperature-dependent term, see figure 7.4. The data points corresponding to the different temperatures lie along a single line, which means that the used method to describe the reaction rate as a product of a temperature-dependent term and a p_w/p_{eq} term is valid.

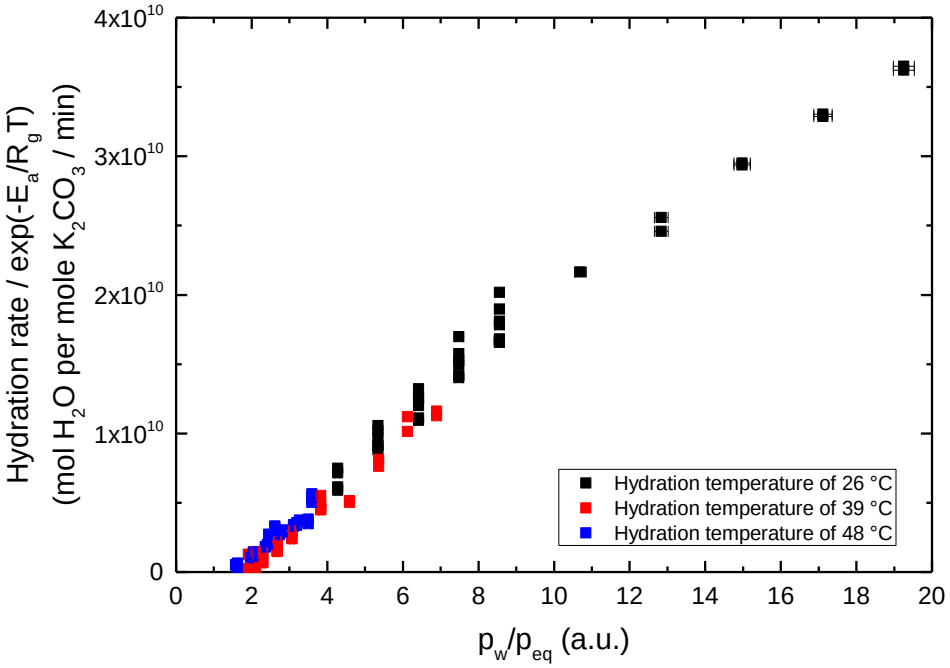

Figure 7.4. Master curve describing the hydration process. The fact that the data points corresponding to the different temperatures lie along a single line implies that the Arrhenius analysis is justified.

7.2 Dehydration

Dehydration experiments are performed in the following way: potassium carbonate is hydrated at 26 °C and a water vapor pressure of 12 mbar. Then, the temperature is increased to 57 °C, where the sample is still hydrated. Next, the vapor pressure is changed to the desired magnitude and dehydration occurs. The above is repeated for different water vapor pressures. To exclude the impact of any eventual effects caused the history of the sample, the subsequent experiments are not performed by increasing pressure, but also sometimes by lowering pressures. The experiment is repeated under similar conditions using a second sample, existing of particles manufactured by Alfa Aesar. The results plotted as a function of the vapor pressure are shown in figure 7.5.

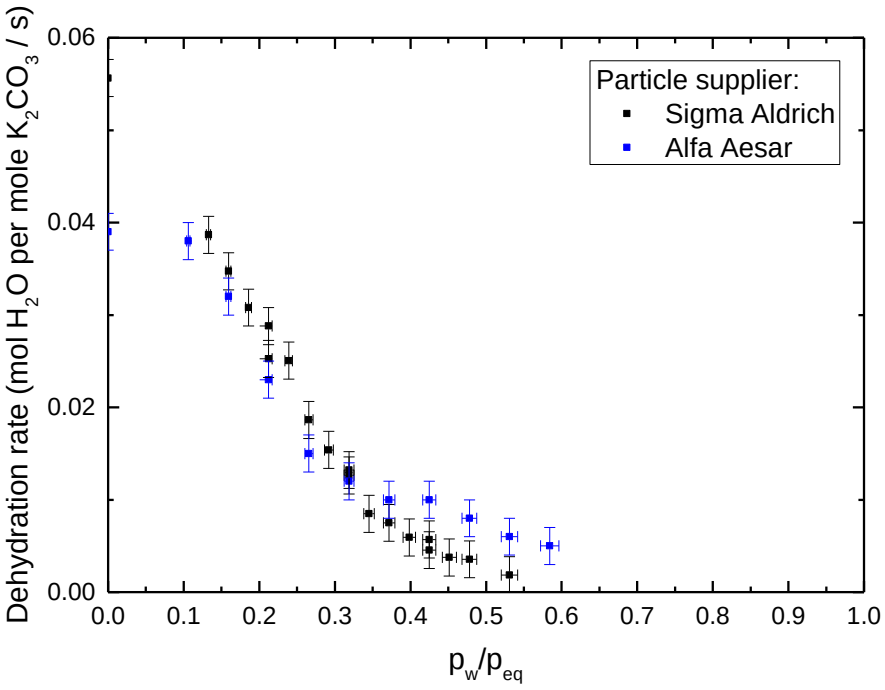

Figure 7.5. Dehydration rate as function of the water vapor pressure at 57 °C.

Both samples show similar behavior: the reaction rate decreases exponentially when increasing the water vapor pressure. Dehydration does not occur for water vapor pressures close to the equilibrium value, which is similar to observations made from the hydration experiments .It would be interesting to test this relationship for different temperatures so comparable analysis to the hydration experiments can be performed, but this was not possible in the used setup.

The dehydration rate observed by Stanish and Perlmutter decayed faster compared to the rates observed in this project [15]. Stanish and Perlmutter observed no dehydration anymore around $p_w/p_{eq} \approx 0.3$, while the experimental data in figure 7.5 shows a dehydration rate until $p_w/p_{eq} \approx 0.55$. Literature study about salt dehydration results in two different behaviors of the dehydration process as function of the water vapor pressure. Exponential decay of the dehydration is observed by $Mg(HCO_2)_2 \cdot 2H_2O$, $Co(HCO_2)_2 \cdot H_2O$ and $CuSO_4 \cdot 5H_2O$ [39-42]. The Topley-Smith effect, observed for $LiSO_4 \cdot H_2O$ [43], where the shows an increase in rate after decreasing rapidly, is not observed for potassium carbonate. For more information about this effect one is referred to Appendix E.

8 Conclusions & outlook

8.1 Conclusions

Potassium carbonate does not form any unwanted reaction products during hydration-dehydration cycling, making it a stable system. This, together with the high storage density of 1.43 GJ/m^3 and practical working conditions potassium carbonate a promising material to be used as a heat storage material. When storing potassium carbonate in the presence of CO_2, $KHCO_3$ is formed. No formation of potassium bicarbonate is observed during the experiments, only during storage. This reaction product dissociates when heating at 93 °C. No other side-products are observed in this project.

Cyclic behavior of potassium carbonate is investigated using isothermal and temperature cycling experiments. Both the hydration and dehydration rate increase asymptotically as a function of experienced cycles. Small particles reach this state faster compared to larger ones. The dehydration process is relative more favored by cycling compared to the hydration process. Also, the relative increase of dehydration rate corresponding to the large particles is higher compared to smaller ones. A similar behavior for the hydration process is not observed.

The hypothesis describing the stabilization process is as follows: when a potassium carbonate sesquihydrated particle is dehydrated it shrinks in size. During the followed rehydration the particle increases in size due to the water uptake. However, its final state is larger than the initial state of the hydrated particle. When dehydrating again, the particle shrinks, but not as much as it did before: the distance between the grains is increased. This favors the water transport within the particle and thus increases the reaction rate.

The water vapor pressure dependencies of both the hydration and dehydration processes are investigated. Both processes do not occur at water vapor pressures close the equilibrium water vapor pressure. Under these conditions, the nucleation process is possibly the limiting factor: the nucleation rate becomes significant at water vapor pressure far enough of the its equilibrium according to the classical nucleation theory.

The hydration rate is described as a product of a temperature-dependent term and a driving-force term. The temperature-dependent term is approximated by Arrhenius analysis and fitting the experimental data resulted in an activation energy of (98 ± 2) kJ/mol K_2CO_3.

8.2 Outlook

In this section, a number of remaining questions regarding the topics investigated in this project are listed.

Firstly, the morphologic changes and their impact on the water vapor transport within the particle can be investigated in more detail. It is unclear why the dehydration is relative more favored by cycling compared to the hydration process. Measuring for example the change in porosity during cycles gives more quantitative results and might lead to new insights.

For practical purposes, it is important to start with the optimized material, without the need of performing any cycles. For this reason, new ways of stabilization should be investigated. It is also interesting to investigate whether the material remains optimized when it is stored for a longer time (in the absence of CO_2).

More granular particles have a higher reaction speed compared to the particles consisting of more smooth surfaces. It is important to know whether the initial particle morphology impacts the final reaction rate. From the results in this project it remains unclear whether the Alfa Aesar particles eventually reach similar hydration rates as the Sigma Aldrich ones or not. Measuring the Alfa Aesar particles during more cycles will answer this question.

During experiments, no hydration nor dehydration was measured at water vapor pressures close to equilibrium. It would be interesting to check if the process is indeed limited by the nucleation step, which will help improving the model describing the reaction rate. This can be done by starting a reaction using a water vapor pressure further from equilibrium and decreasing it quickly when the reaction is started.

A master curve is obtained from the hydration data, however, the available setup did not allow to evaluate the dehydration process in this way. At higher temperatures, the water vapor pressure has to be very high to keep the sample hydrated. This magnitude of p_w was out of reach using the current setup. By increasing the temperature of the water bad and recalibrating, this problem can be solved.

Finally, it would be interesting to repeat the used analysis for other hydrates. Dehydration data is already available for multiple salts in literature, hydration data is rare.

9 Notation

Symbols:

A:	Area [m^2]
A_0:	Collision frequency [mol/s]
a:	Fitting parameter defined in eq. 2.20 [$mol \cdot s^{-1} \cdot K^{-3/2}$]
b:	Fitting parameter defined in eq. 2.20 [K^3]
C_1:	*N*-independent term defined in eq. 2.12 [J/mol]
C_2:	*N*-independent term defined in eq. 2.12 [$J/mol^{2/3}$]
E_a:	Activation energy [J/mol]
f:	Term dependent of the pressure ratio defined in eq. [-]
G:	Gibbs free energy [J]
$\Delta G^*_{\mathrm{nucl}}$:	Change in Gibbs free energy corresponding to a critical nucleus [J]
ΔG_{bulk}:	Change in Gibbs free energy corresponding to the bulk [J]
$\Delta G_{surface}$:	Change in Gibbs free energy corresponding to the surface terms [J]
ΔG_r:	Reaction Gibbs energy [J/mol]
g_i:	Gibbs free energy of phase *i* [J/mol]
ΔH:	Molar reaction enthalpy [J/mol]
ΔH_w:	Enthalpy change per mole H_2O [J/mol]
ΔH_v:	Reaction enthalpy per unit volume [J/m^3]
h:	Heat transfer coefficient [$W/(m^2 \cdot K)$]
J:	Nucleation rate [mol/s]
k:	Temperature dependent term defined in eq. [mol/s]
k_B:	Boltzmann constant [$J \cdot K^{-1}$]
L:	Loading (mol H_2O per mole salt)
M_i:	Molar mass of *i* [kg/mol]
m_i:	Mass of *i* [kg]
N:	Amount of moles [mol]
N_s:	Number of nucleation sites [-]
p:	Pressure [mbar]
p_w:	Water vapor pressure [mbar]
p_{eq}:	Equilibrium water vapor pressure [mbar]
p_{delq}:	Deliquescence water vapor pressure [mbar]
Q_c:	Heat transfer by conduction [W]
Q_r:	Heat transfer by radiation [W]

Q_d:	Heat needed by reaction [W]
q:	Heat flow [W]
R:	Particle radius [m]
R_g:	Gas constant [$J \cdot mol^{-1} \cdot K^{-1}$]
r_c:	Radius of the unreacted core [m]
r_{nucl}:	Nucleus radius [m]
dr/dt:	Shrinking rate of the unreacted core [m/s]
T:	Temperature [K]
t:	Time [s]
V:	Volume [m^3]
V_{nucl}:	Nucleus volume [m^3]
v_n:	Molar volume of phase *n*
X:	Conversion [-]
Z:	Zeldovich factor [-]
β:	Nucleus growth rate [mol/s]
$\gamma_{m,n}$:	Surface energy between phase *m* and *n* [J/m^2]
$\mu_{s,i}$:	Chemical potential of solid phase *i* [J/mol]
μ_w:	Chemical potential of water [J/mol]
σ:	Stefan-Boltzmann constant [$W \cdot m^{-2} \cdot K^{-4}$]

Abbreviations:

PCM:	Phase change materials
TCM:	Thermochemical materials
TGA:	Thermogravimetric analysis
DSC:	Differential scanning calorimetry

10 References

[1] Van der Veen, G. Environmental accounts of the Netherlands 2009, CBS Statistic Netherlands, 2012, p.1-143.

[2] J. Gerdes, S. Marbus, and M. Boelhouwer. Energietrends, 2016. Technical report, ECN, 2016.

[3] What is Geothermal Energy? (2017, February 3). Retrieved from http://www.thermogis.nl/general_info.html

[4] Weerstation Houten, (2017, April 7). Retrieved from www.weerstation-houten.nl

[5] Colclough S. M., Griffiths P. W. Hewitt, N. J., A year in the life of a Passive House with Solar Energy Store, 2010.

[6] International Renewable Energy Agency (IRENA), IRENA-IEA-ETSAP Technology Brief 4: Thermal Storage, (2013)

[7] Cabeza L.F., Heinz A., Inventory of Phase Change Materials (PCM), IEA (2005)

[8] Hauer A., Thermal energy storage with zeolite for heating and cooling applications, Proceeding of the International sorption heat pump Converence, 2002, Science Press, p. 385-390.

[9] International Critical Tables, Retrieved from www.knovel.com (2003)

[10] Brunold S., Frey R., Frei U., Comparison of three different collectors for process heat applications, Proceedings SPIE – Optical Materials Technology for Energy Efficiency and Solar Energy Conversion XIII, 1994, vol. 2255 (107), p. 1-15

[11] Lele A. F. A Thermochemical Heat Storage System for Households, Springer 2016.

[12] A.J. de Jong, F. Trausel, C. Finck, L. Vliet, R. Cuypers, Thermochemical heat storage – system design issues, (2013) Energy Procedia 48 (309-319).

[13] C.J. Ferchaud, Experimental study of salt hydrates for thermochemical seasonal heat storage, (2016)

[14] G.T. Whiting, D. Grondin, D. Stosic, S. Bennici, A. Auroux (2014) Solar Energy Materials & Solar Cells 128: 289-295

[15] P.A.J. Donkers, L.C. Sögütoglu, H.P. Huinink, H.R. Fischer, O.C.G. Adan, A review of salt hydrates for seasonal heat storage in domestic applications. (2017)

[16] M.A. Stanish, D.D. Perlmutter, Kinetics and Transport Effects in the Dehydration of Crystalline Potassium Carbonate Hydrate, (1983) AlChE Journal (Vol. 29, No. 5)

[17] M.A. Stanish, D.D. Perlmutter, Rate Processes in Cycling a Reversible Gas-Solid Reaction, (1984) AlcChE Journal (Vol. 30, No.1)

[18] M.A. Stanish, D.D. Perlmutter, Kinetics of Hydration Dehydration Reactions Considered As Solid Transformations, (1984) AlcChE Journal (Vol. 30, No.4)

[19] N.F.H. Bright, W.E. Garner, J. Chem. Soc. (1934), p. 1872

[20] J.A. Cooper, W.E. Garner, Proc R. Soc. London, Ser. A, 174 (1940), p. 487

[21] Kaschiev, D. Nucleation, Elsevier (2000), p. 184-223.

[22] Butt H., Graf K., Kappl M., Physics and Chemistry of Interfaces, WILEY-VCH (2006)

[23] Levenspiel O. Chemical reaction engineering, Wiley, 1999.

[24] P. Atkins, J. de Paula, Atkins' Physical Chemistry, Oxford university press (2010)

[25] L. Greenspan, Equilibrium Relative Humidity, Saturated Salt Solutions. (1976)
[26] van Essen V.M, Zondag H.A., Schuitema R., van Helden W.G.J., Rindt C.C.M., Materials for thermochemical storage: characterization of magnesium sulfate, Proceedings conference Eurosun, 2009.
[27] van Essen V.M, Zondag H.A.,L.P.J. Bleijendaal, B.W.J. Kikker, M.Bakker, Appication of MgCl2*6H2O for thermochemical seasonal solar heat storage, 5th International Renewable Energy Storage Conference, 2010.
[28] R.L. Lehman, J.S. Gentry, and N.G. Glumac, Thermal stability of potassium carbonate near its melting point, Thermochim. Acta, vol.316, pp.1-9, 1998.
[29] D.D. Wagman, W.H. Evans, V.B. parker, R.H. Schumm, I. Halow, S.M. Bailey, K.L. Churney, and R.L. Nuttal, The NBS tables of chemical thermodynamic properties, J. Phys. Chem. Ref. Data, vol 11, no. 2 p.302, 1982.
[30] R. Byron Bird, Warren E. Stewart, Edwin N. Lightfoot, Transport Phenomena, John Wiley & Sons, (2007)
[31] Convective Heat Transfer Coefficient Table (2017, April 6). Retrieved from http://www.engineersedge.com/heat_transfer
[32] Holzner S., Physics for Dummies, Wiley Publishing inc. (2006)
[33] Mutin J.C., Watelle G., Study of a Lacunary Solid Phase II-Morpholicial and Kinetic Characteristics of its Formation. Journal of solid state chemistry 28 (1979) 1-12.
[34] Rammelberg H.U., Schmidt T., Ruck W., Hydration and dehydration of salt hydrates and hydroxides from thermal energy storage – kinetics and energy release, Energy Procedia 30 (2012) 363-369.
[35] Sögötoglu L.C. performed the IR-spectroscopy, (2017).
[36] OATAO, Open Archive Toulouse Archive Ouverte, (2017, 21 March), Retrieved from http://dx.doi.org/10.1016/j.supflu.2009.03.008.
[37] Mackaij M.B. Reaction Kinetics and Morphologic Changes During Hydration of K_2CO_3. TNO (2017)
[38] Peng Y., Wang F., Wang, Z., Alayed A.M., Zhang Z. Yodh A.G., Han Y. Two-step nucleation mechanism in solid-solid phase transitions, (2014), Nature Materials DOI: 10.1038/NMAT4083.
[39] The Effect of the Water Vapor Pressure on the Kinetics of the Thermal Dehydration of Some Hydrates. Examples of Magnesium, Manganese, Cobalt, Zinc, Yttrium and Erbium Formate Dihydrates, Masuda Y. Netsu Sokutei (1995).
[40] Anisotropic Solid-State Reaction. Dehydration of Manganous Formate Dihydrate. Eckhardt R.C., Flanagan T.B. University of Vermont (1964).
[41] The Dehydration of Salt Hydrates. Colvin J., Hume J. (1938).
[42] Dependence of Kinetics of Copper Sulfate Pentahydrate Dehydration on Water vapor Pressure. Lyakhov N.Z., Chupakhin A.P., Isupov V.P. Boldyrev V.V. Journal of solid state chemistry 26, 173-178 (1978)
[43] Effect of water vapor pressure on thermal dehydration of lithium sulfate monohydrate. Seto Y., Sato H., Masuda Y. Elsevier (2002).
[45] Topley B, Smith ML (1931) Nature 128:302
[46] L'vov B.V. (2007) Springer 100-105
[47] Topley B, Smith ML (1935) J Chem Soc 321–325
[48] Volmer M, Seydel G Z. (1937) Phys Chem A179:153–171
[49] Bertrand G, Lallemant M, Mokhlisse A, Watelle-Marion G (1978) J Inorg Nucl Chem 40: 819–824

11 Appendix

Appendix A: TGA Calibration

The water vapor pressure inside the TGA setup is controlled by mixing wet air together with dry air in certain ratios. This mixture is blown into the TGA setup using an airflow speed of 300 mL/min. The mixing is controlled by use of a computer. The vapor pressure inside the TGA setup is calibrated using various salts and corresponding deliquescence relative humidities (DRH) found in literature [25], see figure A.1. p_{deliq} denotes the deliquescence water vapor pressure from literature, while x denotes relative amount of water in the mixture, this is the adjustable parameter for controlling the mixture water vapor pressure inside the TGA.

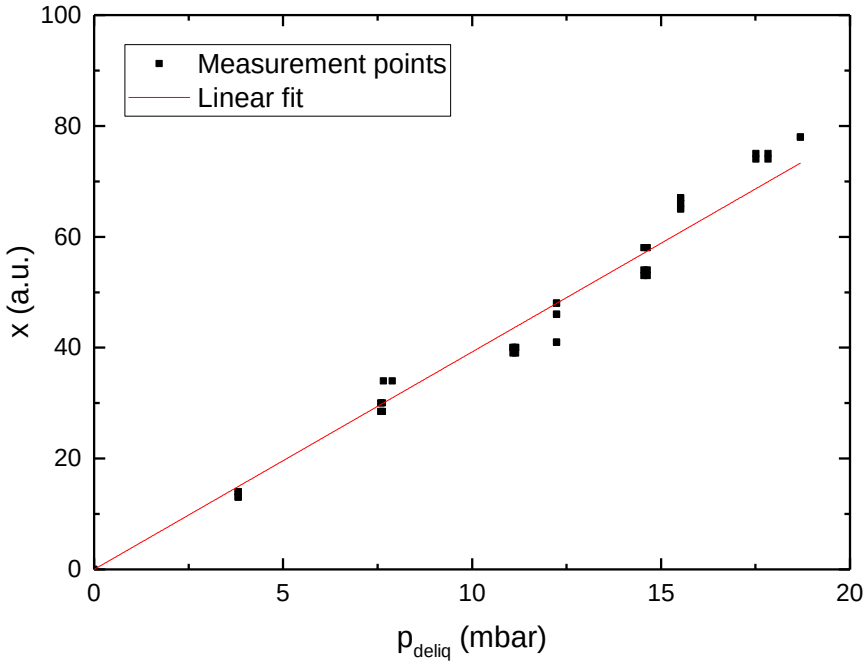

Figure A.1. Water vapor pressure calibration inside the TGA setup.

From figure A.1 one observes a linear behavior between humidity and pressure. The corresponding fit is given by:

$$x = (3.92 \pm 0.04) p_{deliq}, \qquad (A.1)$$

where p_{deliq} is in mbar. The used salts are: lithium chloride, magnesium chloride, potassium acetate, potassium carbonate and magnesium nitrate.

Appendix B: Error approximation

The error corresponding to the loading is approximated by measuring the loading of a sample in its steady state, see figure A.2, which is part of the measurement from figure 5.1. From this figure, the experimental error of the loading is estimated as 0.002 mol H_2O per mole K_2CO_3.

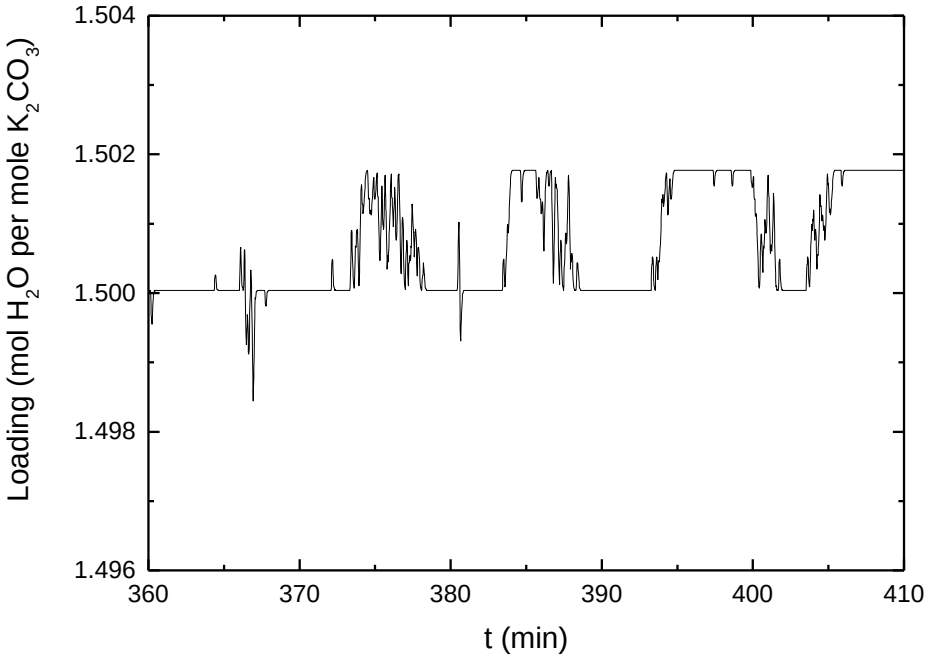

Figure A.2. Fluctuations in loading of a sample in its steady state. The experimental error is estimated as 0.002 mol H_2O per mole K_2CO_3.

Appendix C: Flow-rate

Changing this flow rate has influence on two aspects: firstly, the amount of water molecules the particles see. When using a too low flow rate, the amount of available water molecules in the air will be the limiting factor for the reaction speed. To draw any conclusions from experiments which investigate the dependency of the reaction rate on the vapor pressure, it is important that the air flow will not be the limiting factor. Secondly, when working at higher temperature, the air flowing into the system is a bit cooler than the environment. In this way, the imposed temperature will not always be reached. As visible in figure A.3, a higher flow rate results in a lower sample temperature.

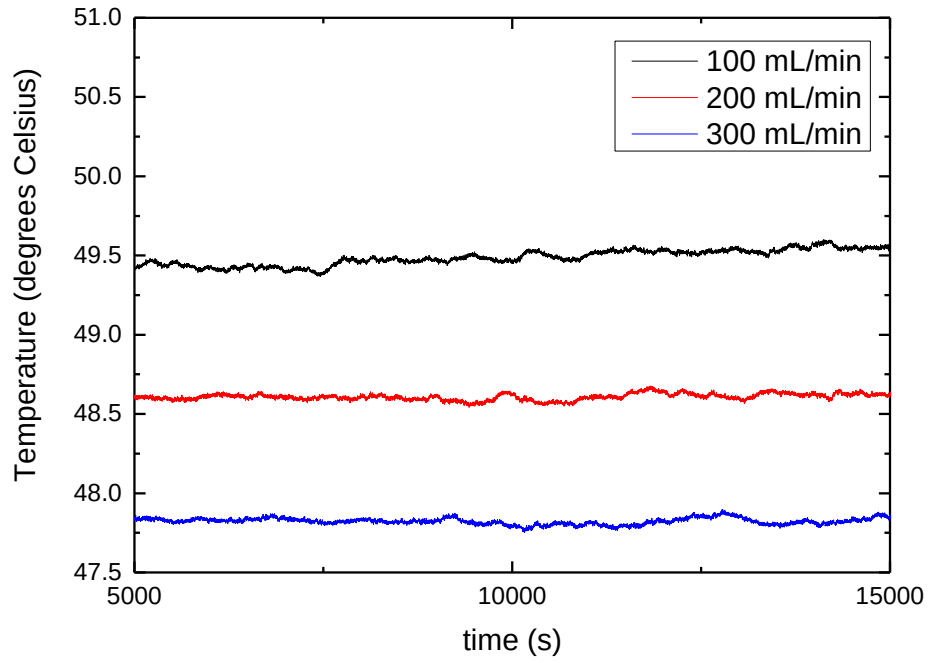

Figure A.3. The influence of the flow rate on the sample temperature. The imposed temperature is equal to 50°C.

Isothermal experiments using small particles are performed with three different flow rates: 100 mL/min, 200 mL/min and 300 mL/min, see figure A.4. Dehydration and hydration occurs at a water vapor pressure of 0 and 12 mbar respectively.

With increasing the flow rate, the dehydration process speeds up. However, when purely looking at the temperature difference, one would expect that the dehydration process slows down when using a higher flow rate. Since this is not the case one concludes that the air surrounding the particles did not refresh fast enough and thus the limited the dehydration process.

The hydration process also speeds up using higher flow speeds. The cause of this effect can be a combination of both aspects. Since a higher flow speed means more water molecules that can react, but also implies a lower temperature and thus faster hydration, the main cause of difference in reaction rate is unknown.

The experiments in this project are performed using a flow rate of 300 mL/min.

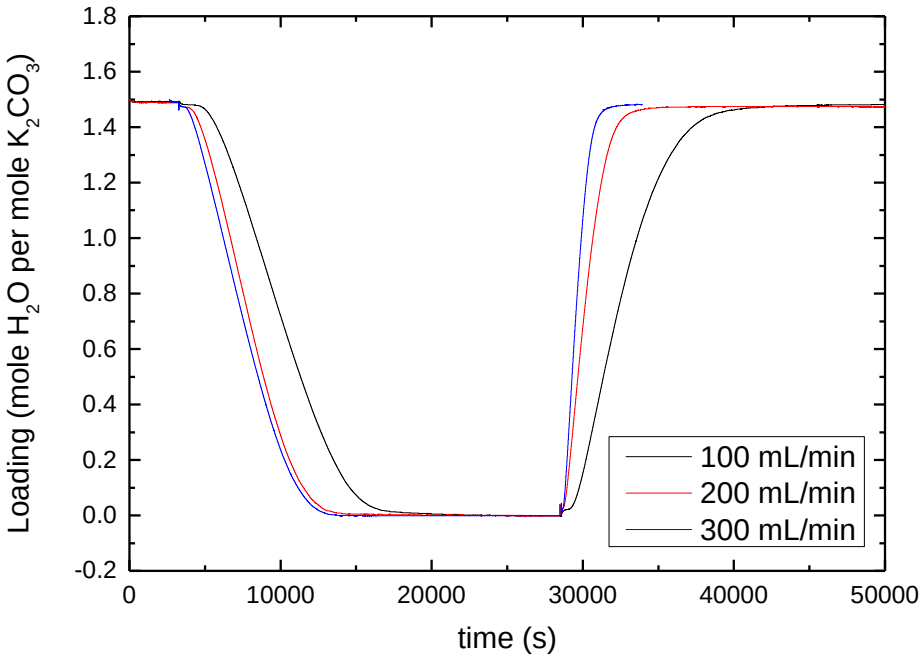

Figure A.4 The influence of the flow rate on the reaction speed. Isothermal experiment using small particles, imposed temperature of 50°C.

Appendix D: Derivation of the Clausius-Clapeyron equation

For a two phases system the change in Gibbs free energy is given by [24]:

$$dG_a = V_a dp - S_a dT, \tag{A. 2}$$

and

$$dG_b = V_b dp - S_b dT, \tag{A. 3}$$

where V_a denotes the molar volume of phase a and S_a the molar entropy. When both phase a and b are in equilibrium the change in Gibbs free energy is equal, resulting in:

$$V_a dp - S_a dT = V_b dp - S_b dT. \tag{A. 4}$$

Rearranging leads to:

$$\frac{dp}{dT} = \frac{\Delta S}{\Delta V}, \tag{A. 5}$$

where $\Delta V = V_a - V_b$ and $\Delta S = S_a - S_b$. In equilibrium the total change in Gibbs free energy is zero, which means:

$$\Delta G = \Delta H - T\Delta S = 0, \tag{A. 6}$$

and therefore:

$$\Delta S = \frac{\Delta H}{T}. \tag{A. 7}$$

Substituting this relationship results in the Clapeyron equation:

$$dp = \frac{\Delta H}{\Delta V}\frac{dT}{T}, \tag{A. 8}$$

When the considered phase transition is between a gas phase and a liquid or solid, the volume of the gas exceeds greatly the volume of the condensed phase and thus:

$$\Delta V \approx V_{gas} = \frac{R_g T}{p}. \tag{A. 9}$$

Here R_g denotes the gas constant, the vapor is assumed to be ideal. This substitution results in the differential form of the Clausius-Clapeyron equation:

$$\frac{dp}{p} = \frac{\Delta H}{R_g}\frac{dT}{T^2}. \tag{A. 10}$$

Assuming the change in molar enthalpy does not vary with temperature nor pressure, this relationship can be integrated resulting in:

$$\ln\left(\frac{P_1}{P_2}\right) = \frac{\Delta H_{vap}}{R_g}\left(\frac{1}{T_2} - \frac{1}{T_1}\right). \tag{A. 11}$$

This relationship is useful to make phase-diagrams. By using some data points and extrapolating, a p-T diagram is made responding to K_2CO_3, see figure 1.3.

Appendix E: Topley-Smith

When dehydrating a crystalline hydrate, the dehydration rate is expected to be dependent on the prevailing water vapor pressure p_w. The first thought is that the rate decreases with increasing p_w. However, a less trivial change in rate is observed: the dehydration rate initially decreases very rapidly with increasing p_w, reaches its minimum and starts increasing. After reaching a certain maximum, the dehydration rate starts decreasing again. This effect was observed for the first time by Topley and Smith in 1931 [45]. Since then, the T-S effect has been found on many other hydrated salts. A list of 26 crystalline hydrates is made by L'vov B.V. [46].

No physical explanation for this effect is accepted yet. Next, two possible explanations are discussed. More theories are available, but at present the recrystallization theory has the widest acceptance. Also, the theory based on the existence of a spatial gradient of temperature in the reaction zone has quite some support. The latter one can be modelled with varying degrees of success [46].

Recrystallization

During dehydration at very low vapor pressures, the water molecules are able to leave the interface through narrow capillaries of the particle. At a slightly higher p_w, the transport through these capillaries is more difficult, because water may be adsorbed on the walls of these channels. When the water vapor pressure becomes high enough, the reactant is able to recrystallize, resulting in additional cracks, channels and pores to promote water transport. At even higher values of p_w, the importance of the reverse reaction comes into play. The total dehydration rate will decrease and eventually become zero when the equilibrium value for the vapor pressure is reached [48].

Temperature gradient

This theory only explains the rise of dehydration rate with increasing p_w, the reason for the initial decrease of the reaction rate remains unclear. Thermal conductivity increases with increasing p_w, due to improved conduction. When the thermal conductivity increases, the material experiences less self-cooling and the dehydration process is favored. This only happens until the average free path length of the water molecules approaches the value of the distance between powder grains, which explains the maximum of the dehydration rate [49].